A Study of Velocity-Dependent JND of Haptic Model Detail

by

John Ko-Han Tang

A thesis
presented to the University of Waterloo
in fulfillment of the
thesis requirement for the degree of
Master of Applied Science
in
Electrical and Computer Engineering

Waterloo, Ontario, Canada, 2010

I hereby declare that I am the sole author of this thesis. This is a true copy of the thesis, including any required final revisions, as accepted by my examiners.

I understand that my thesis may be made electronically available to the public.

Abstract

The study of haptics, or the sense of touch in virtual reality environments, is constantly looking for improvements in modeling with a high fidelity. Highly detailed models are desirable, but they often lead to slow processing times, which can mean a loss of fidelity in the force feedback sensations. Model compression techniques are critical to balancing model detail and processing time. One of the proposed compression techniques is to create multiple models of the same object but with different levels of detail (LOD) for each model. The technique hypothesizes that the human arm loses sensitivity to forces with the increase of its movement speed. This the compression technique determines which model to use based on the user's movement speed. This dissertation examines studies how the movement speed of the user affects the user's ability to sense changes in details of haptic models.

Experiments are conducted using different haptic surfaces. Their levels of detail are changed while the subject interacts with them to mimic the effects of a multiresolution compression implementation. The tests focus on the subjects' ability to differentiate changes of the surfaces at each speed. The first experiment uses curved surfaces with multiple resolutions. This test observes the sensitivity of the user when the details on the surface are small. The results show that the subjects are more sensitive to changes of small details at a lower speed than higher speed.

The second experiment measures sensitivity to larger features by using trapezoidal surfaces with different angles. The trapezoidal surfaces can be seen as a low-resolution haptic model with only two vertices, and changing the angles of the trapezoids is seen as changing the radii of curvature. With the same speed settings from the first experiment applied to the subjects, the sensitivity for changes in curvature is predicted to decrease with the increase of speed. However, the results of this experiment proved otherwise.

The conclusions suggest that multiresolution designs are not a straightforward reduction of LOD, even though the movement speed does affect haptic sensitivity. The model's

geometry should be taken into account when designing the parameters for haptic model compression. The results from the experiments provide insights to future haptic multiresolution compression designs.

Acknowledgements

I want to first thank my supervisor, Professor David Wang, for the support and guidance he offered throughout my studies.

I thank both the Natural Science and Engineering Research Council (NSERC) and my industrial sponsor, SysCor Controls & Automation, for their financial contributions towards my degree.

I would also like to thank Dr. Mehrdad Zadeh for his valuable input on the construction of the experiments and analysis of the data. Also, all the volunteers, my fellow researchers, and the friends at University of Waterloo have my greatest gratitude for their time and knowledge shared to make the experience invaluable.

Last but not least, I want to express much thanks to my parents Pei-Chong and Lynn for all the support, motivation, and patience they have provided over the three years.

Table of Contents

List of Tables **x**

List of Figures **xiii**

1 Introduction **1**

1.1 Haptic Model Compression 3

1.2 Thesis Outline 5

2 Background **7**

2.1 Kinesthetic Feedback and Haptic Devices 8

2.1.1 Kinesthetic Feedback 8

2.1.2 Haptic Devices for Kinesthetic Feedback 10

2.2 Virtual Models 14

2.2.1 Mesh Model 15

2.2.2 Haptic Rendering 18

2.3 Compression Techniques 20

2.3.1 Multiresolution Models 21

2.3.2 Adaptive Sampling 23
2.3.3 Deadband Transmission 24
2.4 Psychophysic Threshold and JND 25
2.4.1 Classical Psychophysical Theory 26
2.4.2 Theory of Signal Detection and Application 31
2.5 Analysis of Variance 37
2.5.1 Two-Way ANOVA for Repeated Measures 37

3 Experimental Design **40**
3.1 Overview 40
3.2 Kinesthetic Feedback Devices 41
3.3 Graphical Display 43
3.3.1 Graphical User Interface 44
3.3.2 Speed Indicator 44
3.4 Experimental Procedure 45
3.4.1 Subject Training 46
3.4.2 Experimental Phase 48

4 Experiment One: JND of Resolution **53**
4.1 Hypothesis 53
4.2 Method 54
4.2.1 Surface Definition 54
4.3 Participants 58

4.4 Results 58
4.5 Conclusion 63

5 Experiment Two: JND of Declination **66**

5.1 Hypothesis 66
5.2 Method 67
5.3 Participants 69
5.4 Results 69
5.5 Conclusion 74

6 Conclusion and Future Research **77**

6.1 Future Recommendations 78

Appendices **82**

A Experimental Results **82**

B Surface Properties of Experiment One **88**

References **95**

List of Tables

2.1 Example of Method of Limits 30

2.2 Example Results of Yes-No Method 33

2.3 Example of Repeated Measures 38

2.4 Example of Two-Way ANOVA 38

3.1 Haptic Device Specifications 42

4.1 Table of Average Results from Experiment One 60

4.2 Table of Trends 60

4.3 JND Sorted by Applied Force 62

5.1 Results of Experiment Two 71

5.2 JND After Sorting by Applied Force 71

A.1 Resulting JND from Experiment One 83

A.2 ANOVA Table for Speed and Surface 83

A.3 Average Applied Force from Experiment One 84

A.4 Resulting JND from Experiment Two 85

A.5 ANOVA Table for Speed and Surface 86

A.6 Average Applied Force from Experiment One 87

B.1 Table of Conversion for Experiment One 89

List of Figures

1.1 A VE Setup 3

1.2 The Processes of A Haptic Loop 4

2.1 A Teleoperation Setup 9

2.2 The Anthropomorphic Robot Designs 12

2.3 The Delta Robot Designs 13

2.4 The Multi-Digit Robot Designs 14

2.5 Example of Mesh Model 16

2.6 Example of Deformable Model 18

2.7 Example of God-Object 21

2.8 Example of Multiple LOD 23

2.9 Example of Deadband Transmission 25

2.10 Example of Ogive Curve 28

2.11 Example Plot of Yes-No Method 34

2.12 Example of 4AFC 34

2.13 Example of FCT Plot 36

3.1 Twin-Bar Target for Speed Control 46
3.2 Colours of Speed Indicator 47
3.3 Example of Experimental Setup 48
3.4 Training Interface 49
3.5 Test Procedure Timing 52

4.1 Screenshot of Experiment One 55
4.2 Surface Definition of Experiment One 56
4.3 Sample FCT Plot for Experiment One 59
4.4 Results of Experiment One 61
4.5 JND Sorted by Applied Force 63
4.6 Grouped JND Sorted by Applied Force 64

5.1 Surface Definition 68
5.2 Screenshot of Experiment Two 68
5.3 Decrease of Curvature 69
5.4 Sample Data of Experiment Two 70
5.5 Results of Experiment Two 72
5.6 JND After Sorting by Applied Force 73
5.7 Grouped JND After Sorting by Applied Force 73
5.8 Static Touch Configuration 75
5.9 Curves with Different Length 76
5.10 Moving Single Point Contact to Imitate Multi-Touch 76

6.1 Different Methods of Defining The Vertices of A Model 80

Chapter 1

Introduction

Incorporating the sense of touch in an interactive virtual environment is the next frontier towards achieving digital realism. For decades, computer users have viewed computer generated graphics on monitors, and the level of interactivity with those virtual objects has increased rapidly. This can give application areas such as medical research, industrial design, and architectural engineering a major advantage in the training and/or simulation process. It is only recently that researchers have looked into adding the sense of touch, or *haptic feedback*, into the user's virtual experience.

Traditionally, operators of a virtual environment (VE) use passive interfaces such as the mouse, keyboard, or joystick for input. Users usually rely on visual and audio cues to assess their surroundings and react to them. To improve the user's spatial perception, "haptic" feedback can be added to the existing set of sensory feedbacks. The word "haptic" refers to the sense of touch. E.H. Weber is one of the first researchers to study the sense of touch (amongst other senses)[46]. Haptics have been traditionally studied with physical objects to create either tactile or weight stimulation [33] [5], but recent advancements in robotics have started trends to use robots to simulate haptic surfaces [47]. Using robots may be more difficult to construct than simple objects for studying haptics, but they are much

more versatile, dynamic, and the experiments are highly repeatable. This leads to studies of incorporating those robotic devices into virtual simulations for generate haptic sensation and to enhance the overall virtual experience for users. For example, in Kim et al.[21], a haptic interface is used to implement realistic training for laparoscopic surgery[1]. The trainees' performances are rated by their time-to-completion, push accuracy, cut accuracy, and tool control. Kim discusses the resulting improvement of performances with haptic feedback against the performances without haptic feedback. The trainees' performances increased by almost 100% with the use of haptics.

In Figure 1.1, a typical haptic-feedback-integrated workstation is shown. Through the sensors on the haptic device, the user's position is fed to the virtual environment for update. This data is then given to the physics process in the workstation to calculate appropriate interactions, such as making contact with a model or picking up an object. The physics process then calls on the haptic and graphics processes for providing proper force and visual information to be fed back to the user through appropriate peripheral devices.

There is a strong association between visual and haptic feedback in the human sensory process. Feygin et al.[9], studied the learning curve of human arm motion by having the subjects trace 3-dimensional trajectories set by virtual guides. The learning part of the experiment was conducted by having the subject watch the haptic device as it moved along the trajectory (pure visual feedback), having the subject hold the device as it moved while the device was hidden in view (pure haptic feedback), or holding the device while in view also (visual and haptic feedback). No monitor or other display devices were used. The subject was then asked to recall the trajectory by either pure haptic guidance or with visual guidance. The experiments compared the errors obtained for each training-recall

[1]Laparoscopic surgery is a minimally invasive surgery (MIS) where robotic arms are inserted through small incisions at the patient's abdomen. The surgery is typically guided by a camera that is also inserted with robot arms. Therefore the surgeon relies on visual feedback to perform the operation. MIS drastically reduces blood loss and speeds up recovery time, in contrast with the traditional open-cavity surgery [31].

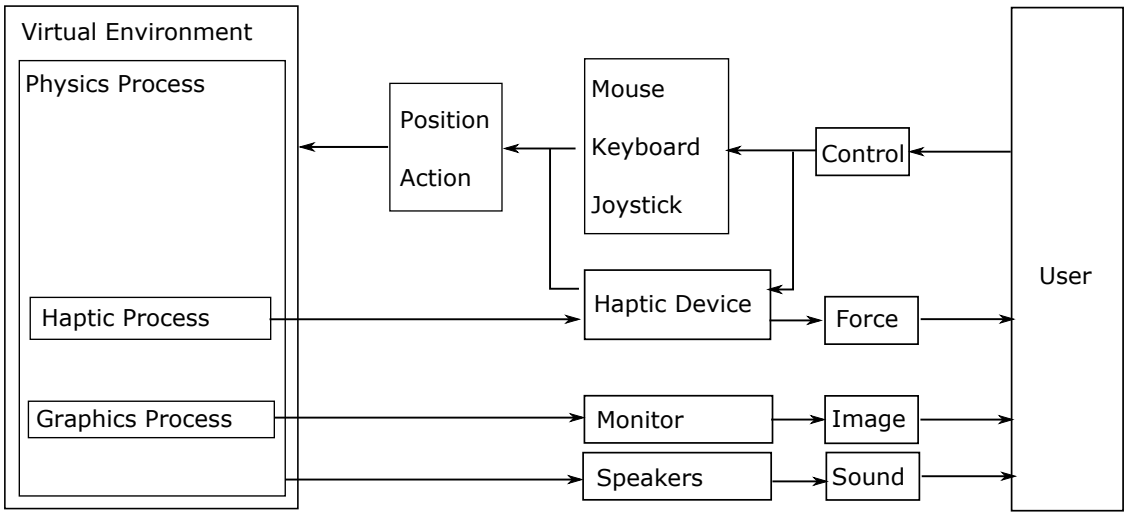

Figure 1.1: Interactivity between user and virtual environment through different interfaces.

combination and saw much improvement with spatial cognition when visual feedback was used with haptic feedback.

1.1 Haptic Model Compression

When creating a haptic model, the amount of detail contained in the model, such as physical features and mechanical structure, is always a concern. Models contain a finite number of data points for the construction of discrete surfaces. Ideally, a model represented by discrete surfaces should have an infinite number of data points to accurately model the fine details of real-life objects, such as smooth curves. However, this concept is impossible to achieve as the computational time is scaled proportionally with the complexity of the model, mainly due to the *collision detection* part of the haptic process, as shown in Figure 1.2. The collision detection, explained in Section 2.2.2, is a search algorithm that looks for the point of contact between the avatar and a discrete surface at every iteration of the haptic loop. Initial collision algorithms have limited the number of data points to

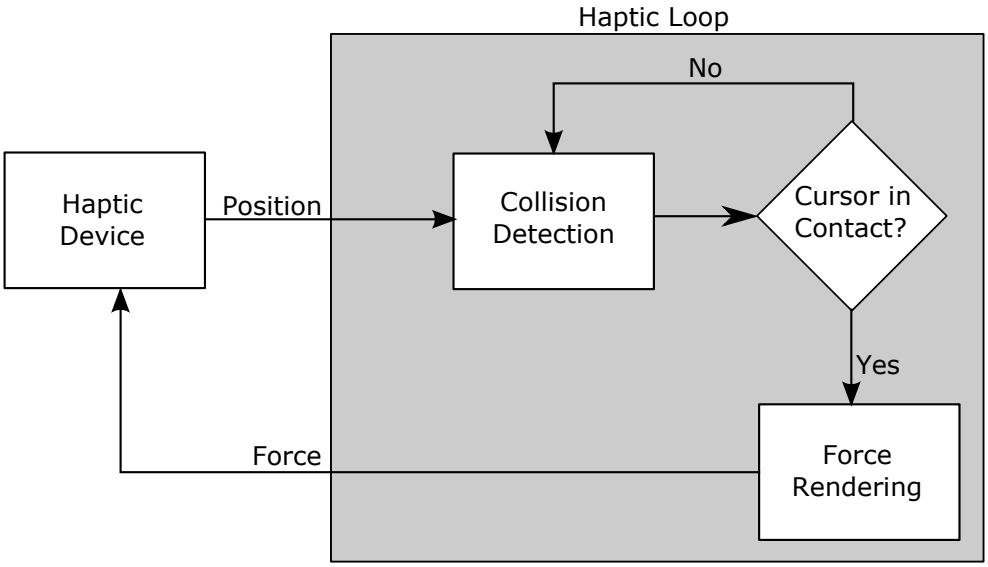

Figure 1.2: The processes of a haptic loop

the hundreds [17]. While better search algorithms have been developed to increase the limit to tens of thousands of data points, this number is still far from being "infinite". To improve the realism of haptic models even further without simply relying on more powerful computing units, haptic model compression methods are being developed.

Hinterseeer et al.[15],[16], introduced a technique called *deadband transmission*. This technique assumes that the average haptic user can not tell the difference between two force levels with small magnitude difference. Therefore, any force below this threshold does not need to be transmitted to the user. By doing so, the average transmission rate of the haptic forces can be reduced. In Kolcarek's thesis [23], an algorithm is developed to combine or split vertices of a mesh model depending on the user's movement speed. The algorithm is based on Hoppe's Progressive Mesh [18] for graphic model rendering. Some of the algorithms involve a multiresolution hierarchy where multiple models are generated for each object for different levels of detail [30],[1].

Using the intuitive idea behind Kolcarek's velocity-driven haptic compression technique

[23], this research investigates human perception in regards to changes in the resolution of haptic models as related to the user's hand velocity. Kolcarek decreased the model's level of detail with the increase of velocity of the *virtual proxy* [2]. In this study, two experiments are conducted to study the relationship between human haptic sensitivity and the velocity of the user's hand movement. The findings on how humans perceive curvatures presented by Pont et al. [33], [32] and Wijntjes et al. [47] provide insight on the design of the haptic surfaces used in the experiments. Zadeh et al has concluded that the human arm's haptic sensitivity decreases with the increase of its speed in experiments that apply aiding and opposing forces relative to the motion of the arm in [49], [50]. Those findings are referenced in the conclusions.

1.2 Thesis Outline

In Chapter 2, the critical background information is presented in the form of a literature review. Section 2.1 discusses current available haptic devices and their designs. Section 2.2 references some techniques employed in creating a virtual environment and its similarities with haptic model rendering. Different techniques for haptic data and model compression are presented in Section 2.3. Section 2.4 introduces some procedures that have been employed in collecting human sensitivity data and discusses how they can be applied in this research.

Chapter 3 explains how the experiments in this research are designed. The haptic device chosen for this research is described in Section 3.2 along with other candidates and their specifications. Section 3.3 shows how the graphical user interface is designed.

[2]Virtual proxy is an abstract object created at the point where the user's avatar, a graphical representation of the user's position in the virtual environment, makes contact with a haptic model. The virtual proxy is used to calculate the feedback force which the haptic device should produce. This is explained in Section 2.2.2.

The procedures of the experiment, including the training of test subjects, are discussed in Section 3.4.

Chapter 4 studies the JND of model resolution with respect to the movement speed. The results show different levels of the subject's movement speed can affect the amount of change in model resolution the subject can detect. The analysis also shows how applying forces higher than the rated force output of the haptic device can skew the results.

In Chapter 5, the study of JND of angle change with respect to the movement speed is presented. The results show the relationship of sensitivity and speed, being opposite to what is hypothesized. Speculations and suggestions for further studies are made to justify this observed behaviour.

Chapter 6 presents the conclusion of experiments performed in this study and how it relates to the objectives. Suggestions for future studies are also made here.

Chapter 2

Background

Certain areas of haptic feedback can be very closely related to how computer graphics (CG) are generated from three-dimensional models, specifically in direct manipulation of virtual models as mentioned in the example from the previous chapter. When the surgeon touches the virtual body with a tool, a certain amount of reaction force on the tool is expected. This reaction force is usually perpendicular[1] to the surface where the contact is made and its magnitude reflects the mechanical properties of the model. When the user sees a cube on the screen, he or she expects to feel the edges of a cube instead of the roundness of a sphere.

This chapter first introduces the haptic devices, specifically kinesthetic feedback devices. The second section explains some of the basic generation, or "rendering", techniques in computer graphics and then compares some of the haptic compression techniques inspired by CG. The next two sections of this chapter introduce psychophysical analysis methods for measuring human sensory limits and explain how they can be used to achieve the objectives of this research. The last section briefly explains how *analysis of variance* can

[1]The orientation of the reaction force can be modified by the *force shading* techniques to remove the discontinuities between discrete haptic surfaces [27].

be used to analyze the significance of the relationship between the control variables and the results.

2.1 Kinesthetic Feedback and Haptic Devices

As introduced in Chapter 1, a haptic device is designed to provide the sensation of touch to its user. Haptic devices can be categorized into two types (some with a combination of both): tactile feedback and kinesthetic feedback. Tactile feedback devices produce sensations felt by the user's skin, such as surface texture and temperature; kinesthetic feedback devices, commonly referred to force feedback, apply forces directly to the user's muscles, joints, and tendons. (While tactile feedback is an equally researched field in haptics, it is not in the scope of this research.)

2.1.1 Kinesthetic Feedback

The ideal design of a kinesthetic feedback device is one that can achieve Newton's Third Law of motion:

> *If a force acts upon a body, then an equal and opposite force must act upon another body*

It means that if the virtual object[2] is rigid and held at a fixed location, then, upon contact with the user's avatar, the device shall immediately output an equal amount of force to counter the force applied by the user to correctly mimic the real reaction force of a stiff object. Similarly, when the avatar breaks the contact, the output force shall immediately

[2]Objects in the virtual environment, such as walls, geometric shapes, and background are referred to as *virtual objects*.

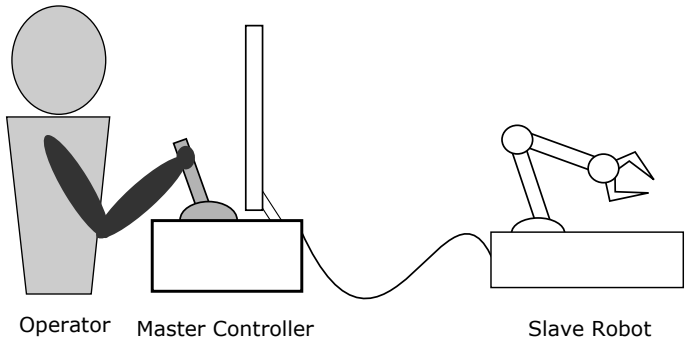

Figure 2.1: An operator controlling a robot via teleoperation. The communication between the master controller and the slave robot can be wired or wireless.

disappear. This requires the device to have a very quick reaction time and a high force output. If the force output is too low, then the incorrect stiffness of the virtual object is conveyed to the user. If the reaction time is too long, then the user will experience sudden transient forces (engage of force) and stickiness (disengage) when coming in and out of contact respectively. Even though there is not yet the technology to achieve this ideal configuration, the limitation on human force-sensitivity only requires the reaction time to be no longer than 1 ms [39]. Compared to the 166 ms average reaction time for human vision sensitivity, the 1 ms is, though very demanding, achievable.

Applications of kinesthetic feedback include interfacing with virtual simulation and teleoperation (Virtual simulation is explained in Section 2.2). In teleoperation, as illustrated in Figure 2.1, an operator controls a slave robot by using master control. If the operator shares the direct line-of-sight with the robot, no additional aides are required for the operator to be aware of the robot's surrounding. When the operator has no direct line-of-sight with the robot, cameras are often added to provide visual feedback to the operator. There are, however, situations where visual feedback is insufficient to provide the operator enough of the robot's surrounding to effectively complete the task. This usually involves tasks that require the robot to manipulate sensitive or fragile objects.

In minimally invasive surgery (MIS), small incisions are made on the patient's abdomen to allow robotic arms to perform surgical operations. This MIS, also known as laparoscopic surgery (for the laparoscope that provides the surgeon video feedback of the operation area), is developed to reduce hemorrhaging during operation and shorten recovery time of patients. In conventional operations, the surgeon relies on the sense of touch as much as sight to perform the surgery. Similarly, with MIS, a video-feed may not provide enough information to the operator as he or she cannot feel the unhealthy tissue such as cancer cells. This is where haptic feedback can provide the operator with another level of awareness to better perform the surgery. By adding position and force sensors at the appropriate locations on the slave robot and active components such as motors on the joints of the controller, the reaction force generated by the slave contacting the body can be permeated back to the operator. The da Vinci® Surgical System from Intuitive Surgical® is such a robot[43].

The design of the kinesthetic feedback device is usually composed of a number of actuators and/or motors for force generation. The force can be transmitted to the user either directly or via a pulley, lever, or gear system for the desired force and/or torque. The serial-link robot is a common design for general purpose, but many others have also been developed for either general purpose or specific applications. The robots are often equipped with an end-effector that mimics a certain tool as an interface for the user. This can be a glove, a type of surgical tool, or a stylus. The user holds on to the end-effector and operates as if it was a real tool, and the robot applies forces to the end-effector according to the user's interaction with the virtual environment.

2.1.2 Haptic Devices for Kinesthetic Feedback

For the last few years, the term "force-feedback" is commonly used to refer to features in consumer electronics such as mobile phones and game controllers. In most cases, the

"force" these devices generate is nothing but vibrations from a motor that spins an off-balance weight. Certain controllers such as the G-series racing wheel from Logitech® provide more specific force-feedback such as resistive steering to simulate the weight the driver feels while operating a vehicle. Although these devices are well-suited for their intended purposes, they are not precise enough for tasks such as surgery simulation and do not provide enough fidelity for general research purpose. Here are some designs of devices that output more precise and consistent forces for kinesthetic feedback.

Anthropomorphic Design

The anthropomorphic robot is one of the more commonly seen robots in haptic researches. The robot has three actuated joints: base, shoulder, and arm, and a ball-joint wrist with which the end-effector is attached. This design provides a minimum of three degrees of freedom (DoF) plus an extra one degree of freedom which the end-effector provides. This design is popular as the dynamics of the robot is well understood. Many of the anthropomorphic designs opt for the *five-bar linkage* design. By doing so, the motors can all be placed at the base to reduce the weight of the arm, which essentially reduces its inertia and the required torque of the base motor. With the anthropomorphic design, the main advantage is the large workspace that it can provide. However, the main weakness lies in its configuration-dependent inertia. The PHANToM® robots take precaution by placing the three motors as close as possible to the base joint to minimize the effect of inertia and driving the joints by wires to reduce friction and backlash. The joints have physical limits built in to avoid singularities.

The PHANToM® series from SensAble™is a good example. The Desktop™and the Omni™are commonly used in haptic research and they are shown in Figure 2.2

(a) The PHANToM Desktop (b) The PHANToM Omni

Figure 2.2: The anthropomorphic robot designs [19], [20]

Delta Design

The delta robot design is commonly used for picking and sorting items in factories for its speed and accuracy. The structure, illustrated in Figure 2.3, has three independently controlled arms joined at the base. The three arms are 120 degrees apart from one another and they each link to a set of parallelograms which join together with a mobile platform. This platform serves as a connector to various end-effectors and it only has translational movement.

Currently available haptic interfaces that use the delta robot design are the Falcon from Novint Technologies, Inc. and various devices from Force Dimension as illustrated in Figure 2.3. These devices boast a high continuous output force of 12 N.

Multi-Digit Design

The designs mentioned previously all have a common shortcoming: they only provide single-point contact for the user. Trying to feel an object with a point contact is similar

(a) Novint Falcon ® with a pistol grip (b) Force Dimension Omega.3

Figure 2.3: The delta robot designs [8], [28]

to exploring a shape with a pen. The general shape of an object cannot be accurately perceived unless the user explores the space at a sufficient speed. Intuitively, when being asked to explore an object by sense of touch, humans will employ all available digits for such a task if possible. Therefore, it is best if a haptic device can provide feedback on all the fingers directly instead of on a stylus. The human hand has roughly 30 degrees of freedom (five fingers with four DoF each plus the palm). Therefore, a system to accommodate all the forces felt by the hand has to be much more sophisticated than the ones mentioned previously.

There are a few available technologies developed for providing kinesthetic feedback on hands, namely the CyberGrasp from CyberGlove Systems and HIRO from the Kawasaki and Mouri Laboratory at Gifu University, Japan. The CyberGrasp system, shown in Figure 2.4b, uses five actuators to create perpendicular forces for each finger by pulling the tips with wires. It needs to be paired up with the CyberGlove system from the same company for sensing the position of the user's fingers. The HIRO III, shown in Figure 2.4a, is a much more complex system with 21 degrees of freedom (fifteen for the fingers and six for the arm). The design is basically a five-digit robotic limb where its "finger-tips" are attached

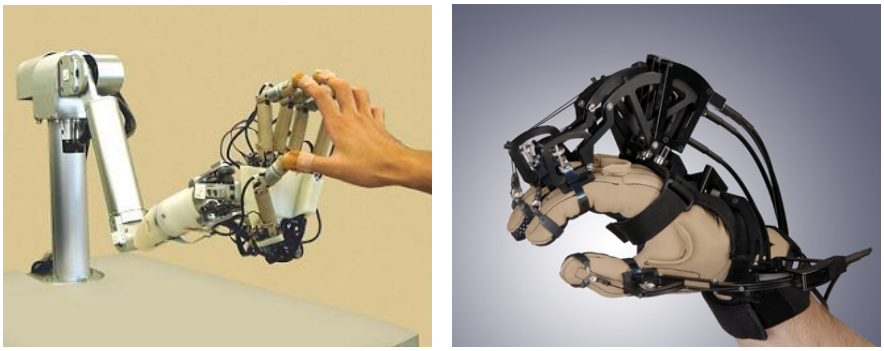

(a) The Haptic Interface RObot, HIRO (b) CyberGrasp™

Figure 2.4: The multi-digit robot designs [44], [25]

to the user's finger-tips.

2.2 Virtual Models

A virtual environment (VE) is a computer-generated "workspace" where virtual objects exist. Conventionally, a VE provides an immersive experience for the user through interactive visuals and sound. With the development and increasing availability of haptic devices, the user experience in a VE has been enhanced with the sense of touch.

A VE is usually interactive through various interfaces, as opposed to computer animation where the user has no control over the content being displayed. Industries such as medical research, geological survey, and computer-aided design (CAD) often implement a virtual environment for their respective simulations as using a VE is a highly repeatable, controllable, and less resource-consuming alternative process than using physical models.

To create these objects so they can be seen and felt in the virtual environment, the digital representation of said objects need to be created. This virtual "model" defines the shape of an object and contains any visual information such as its colour and texture.

These models can be defined by different methods, but the most common one is the mesh model[3]. The architecture and rendering of mesh models are explained in the subsequent sections.

2.2.1 Mesh Model

A model represents a virtual object's appearance in a virtual environment. The most common method for creating a model is to define a number of points in $\Re^3$, or *vertices* on the surface of the object, and then connect neighboring vertices with *edges* to form faces, or *polygons*. When multiple polygons are joined vertex-to-vertex and edge-to-edge to represent a surface or an enclosed volume, a polygon mesh model is formed. The *mesh* refers to the model's appearance of a wire mesh.

The *level of detail* (LOD) is used to describe how similar the digital representation appears to be with its real life counterpart. A model that closely resembles the object it is modeled after means it has a high LOD. The highest LOD is often desired for realism, but often unachievable for complex models as it requires much of the system's resource to generate.

Visual Mesh Model

For a visual model, there are two main components required to create the mesh model, vertex list and polygon list. The vertex list contains the positions of all the vertices of the model, and the polygon list contains the index of each vertex required to form a polygon[4]. A mesh model file may contain lists such as the one given in Table 2.5a

[3]Other methods include Bezier surfaces and Non-uniform rational basis splines (NURBS) [12],[34].

[4]Although the polygon list can sometimes be generated by an automatic process called *tessellation*, it requires the model to be convex and often tweaking is needed. Also, even though there are no restrictions as to the number of edges a face can have, triangular polygons are the most commonly used.

Index	Vertex List	Index	Polygon List	Normal List
0	(0,0,0)	0	(0,1,2)	(0,0,-1)
1	(0,1,0)	1	(1,3,2)	(0,0,-1)
2	(1,0,0)	2	(0,1,4)	(0,-1,0)
3	(1,1,0)	3	(1,5,4)	(0,-1,0)
⋮	⋮	⋮	⋮	⋮
7	(1,1,0)	11	(5,6,7)	(0,0,1)

(a) Lists of vertex, polygon, and normal vectors for creating a cube.

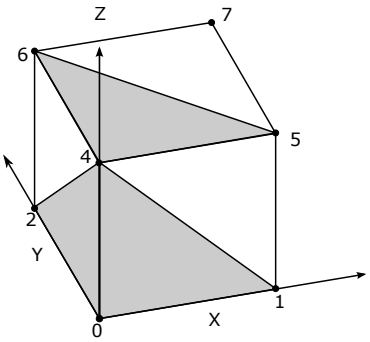

(b) A mesh model of a cube by the data from the table.

Figure 2.5: Lists of vertex, polygon, and normal vectors for creating a cube. The vertex list stores the positions of individual vertices in $\Re^3$. The polygon list stores the index number of all the vertices in each polygon. The normal list stores the normal vector assigned to the polygon with the same index number. For example, the polygon with index of 1 is made up of vertices 1, 3, and 2, and has a normal vector of (0,0,-1). In the figure, the cube is constructed by the polygons, which are alternately shaded with white and gray for emphasis.

There are also components which are optional, yet they are often included in the model file. One of them is the normal vector that defines the front and back of each polygon. There are also processes that can calculate the normals by using the order of the polygon list and their cross-product. The normal vectors are important as they specify how light shall reflect off of each surface. Another optional component is the colour/texture definition, which is used for adding colour or texture mapping to the model.

Haptic Mesh Model

Prior to the introduction of haptic devices in VE's, implementations of real-world physics in virtual simulations existed. Properties such as weight, deformation, and conservation of energy can be used to simulate collisions of objects. The haptic device can use the net force acting on the avatar as it interacts with the environment, calculated by the haptic process, and output to the user. Simply put, a haptic model defines the part of the VE that can be touched by the user.

Mesh models are often also used for haptic applications, and, more often than not, the same model for visual feedback is used for haptic feedback to increase the sense of immersion. An avatar making contact with a virtual cube in the visualization at the same time as the user makes contact with the model via the haptic device heightens the sense of association. By using the same model, much of the model-creation process can be unified as visual and haptic models may share similar properties.

The haptic model contains mechanical properties, such as stiffness and/or surface friction. The stiffness defines the reaction force perpendicular to the particular face, and the friction, both static and dynamic, defines the reaction force along the surface. There are different methods of defining these properties, depending on the realism and complexity required.

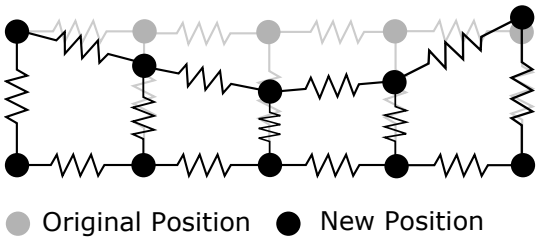

Figure 2.6: A 2D representation of a deformable model, with original and deformed states.

Deformable and Rigid Body Models

Haptic models can be generalized into two categories: deformable and rigid-body, with the latter being the simpler one. In deformable modeling, each vertex is usually assigned a mass and has an initial position instead of a fixed position. The edges that connect the vertices are not of fixed length and have spring and damper constants. A deformable model is simply a network of mass-spring-damper system[5]. The reaction forces on the avatar are calculated by going through all the local reaction forces on each vertex one-by-one.

For a rigid-body model, its shape has no direct relation with its internal forces. Usually rigid-body models are created with the intention of being stiff objects, but softness can be simulated (sometimes unintentionally) with the *god-object* rendering approach. The god-object approach is explained in Section 2.2.2.

2.2.2 Haptic Rendering

After a virtual scene has been created (with a background, a number of objects, and a few light sources), the scene must be *rendered*. This *rendering* process is a set of calculations that convert all the data points from a virtual scene to either graphical planes (vision) or force boundaries (haptics).

[5]This is the linear deformable model.

For graphics, the rendering process produces a 2-D image from the 3-D VE. A viewport, similar to a virtual camera, defines a rectangular frustum with its position, orientation, and field of view. Using the viewport, the renderer calculates model transformations relative to the viewport's axis and light reflections. It compresses the objects within the frustum into a *frame*. For an interactive virtual environment, the rendering process is continuously updating the frames at *real-time* to give the perception of synchronized motion. For vision, a 15 Hz update rate is considered "real-time" [26], but 30 Hz to 60 Hz is a more acceptable refresh rate.

For haptic model rendering, the avatar can be compared to the virtual camera. The virtual camera gathers all the light at a given position in the VE, and the avatar acts similarly with forces. To maintain a high fidelity of the force, the haptic rendering loop runs at a range of 300 Hz to 1000 Hz [7], a much higher rate than the graphics rendering loop. There are mainly two steps in the haptic rendering process, collision detection and force rendering.

Collision Detection

Two objects need to make contact first before any reaction forces can exist between them (except for force fields such as gravity wells, where forces are relative to proximity). If one object has a simple geometry shape that can be defined with a volumetric function, then the contact can be determined by a simple less-than-or-equal-to test[6]. For example, a contact with a sphere is made if the avatar's location relative to the sphere's geometric center is less-than-or-equal-to the sphere's radius. The collision test becomes more complex when arbitrary mesh models are used.

For mesh models, since each one is made up of a number of polygons, the collision detection algorithm is a search algorithm that looks for the polygon closest to the user's

[6]This is considering that the user's avatar is simply a point in space; it has no geometry.

position. The brute-force method is an exhaustive search that goes through every single polygon, checking whether the avatar is above or below the surface. A more common and faster method is to create a hierarchy of spherical boundaries that divides the model [37]. These boundaries become the nodes of a search tree. Gregory et al. [13] added that, since the position of the avatar at a given frame is usually at close proximity of its position from the previous, a better way to search is to start with the tree nodes that are close to the previous location. These techniques allow models of tens of thousands of polygons to be used in haptic scenes. Once contact has been determined, the feedback force can be calculated.

Force Rendering

When the haptic device is considered as "in-contact" with a rigid-body haptic model, a *proxy*, or "god-object", is created on the surface of the polygon. As the proxy penetrates the surface, a spring-damper system is created between the proxy and the god-object. The net force is calculated by Equation 2.1, where $f_N = K_s x + K_d \dot{x}$ in this case (see Figure 2.7). If there is no friction on the surface, then the god-object will always exist on the plane that is closest to the proxy. If the friction coefficient is greater than zero, then the object will remain at the point of penetration until it overcomes static friction.

$$F = f_N(x, \dot{x}, \ddot{x}) + f_F \tag{2.1}$$

2.3 Compression Techniques

With virtual environments becoming more complicated to achieve realism (complex geometry, dynamic lighting, realistic physics, etc.), the rendering process often becomes clogged

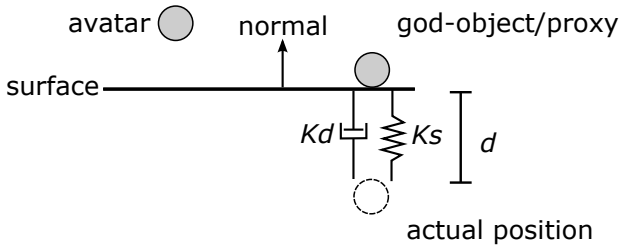

Figure 2.7: An illustration of the god-object method with a spring-damper system.

up with data and struggles to keep up with the user's actions. Solutions include increasing hardware speed, parallelizing the rendering process, or compressing models. While the other two types of solutions deal with technological advances and algorithm optimizations, model compression focuses on the human perception of visual details. The purpose of compression techniques is to reduce the data processed by the renderer without the user noticing the change.

For haptic models, compression techniques need to ensure that, during the change in the model, the user can not feel any change in the haptic sensation. The human haptic sensitivity is much higher than vision, therefore the amount of change between two different LOD models need to be carefully considered. When a mesh model is constructed , there will always exist some discrepancies when modeling an object with a curved surface because it is defined with finite number of points and edges. These discrepancies usually result in difference in surface heights, as shown in Figure 2.8. As the LOD goes down, the difference increases. As mentioned in the previous section on rendering, the force calculation is dependent on contact and distance of penetration.

2.3.1 Multiresolution Models

Section 2.2.1 mentioned that visual models are often used for haptic models as well. For vision, Heok et al.[14] introduced different techniques of changing the amount of level of

detail of mesh models to keep up with a real-time visual frame rate. The simplest is *discrete LOD*, where several models are created for the same object in the preprocess, but with different amount of LOD. In Figure 2.8, a 2-D curve is represented by two "models" of different LOD, with the left one having a higher LOD. During runtime, different models are loaded when certain criteria are met. Not many recalculations are required for this. The *continuous LOD* creates a data structure that allows the specification of an exact number of polygons needed to generate the model during runtime. This provides finer transition and supports progressive transmission. The *view-dependent LOD* deals with predicted behavior of human vision. In a VE scene, less LOD is assigned to objects farther away than objects that are close. View-dependent LOD can also predict where the object of attention is located, and therefore assign less LOD to objects in the user's peripheral vision. The *hierarchical LOD* compensates the shortcoming of the view-dependent LOD, where small objects are overlooked. A hierarchical LOD simplifies objects in groups, and then uses the view-dependent LOD to treat the entire scene as one object.

Essentially, the compression techniques for visual models are giving priority for models that are determined to be objects of focus for the user. Models that are too far away, in motion, or obscured by other objects are, in turn, given a lower priority and therefore given a reduced LOD. The techniques mentioned work best if they can rapidly determine the priority assignment while making sure the transition is unnoticeable for the user. These techniques can be applied to haptic modeling as well, although the criteria for priority assessment are different.

In Zadeh et al.[49], it is mentioned that a human's perception to external forces can be altered by motion. In Zadeh's experiments, the subjects move the end effector of a haptic device at low, medium, and high velocities in separate cases while "opposing" or "aiding" forces are applied to the end effector. (The opposing force is the force applied at the opposite direction of the user's motion, and the "aiding" force is applied along with

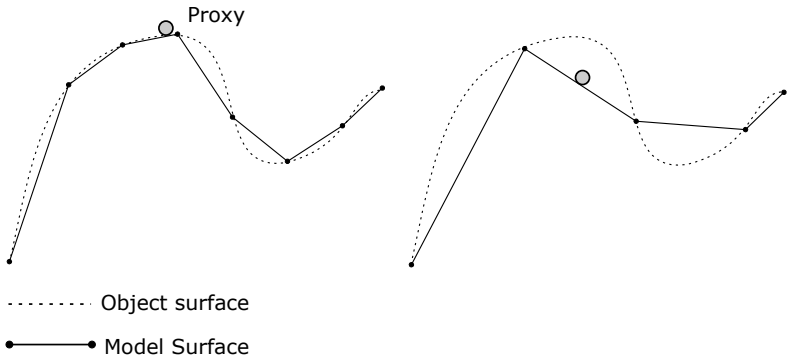

Figure 2.8: An object surface with two models of different LOD

the direction.) The findings show that the subjects are less susceptible to the changes in both opposing and aiding forces (similar magnitude for both directions) as the speed of the subject's hand motion increases.

Kolčárek [23] has implemented a speed-based technique for a multiresolution LOD compression for haptic models. This technique is designed to constantly monitor the user's velocity and change the LOD of the haptic model accordingly. The faster the user moves, the less detail the model has. Similarly, when the user slows down, more and more details are put back into the model. Through user testing, Kolčárek proved his method to be a smooth, continuous transition between high and low LOD models as the users moved on the surface.

2.3.2 Adaptive Sampling

Haptic devices take in position and force data for the rendering process at a fairly fast cycle. For the PHANToM^{TM}devices from SensAble, the default speed for reading in sensor values is 100 Hz [39]. Researchers have argued that this number is usually too high considering the limits of human motion and the Nyquist theory and have proposed an adaptive sampling algorithm to free up data transmission and storage [40]. This adaptive sampling algorithm by Shahabi changes the step size of the sensor loop according to the difference between

the current and previous sensor values. If the absolute difference is greater than a certain threshold, then the step size is increased to accommodate fast motion, otherwise it is decreased for slow movement.

This method is best-suited for haptic devices with a great number of sensors, such as the CyberGlove and HIRO systems. Furthermore, Shahabi also proposes to group sensors of different joints for selective sampling frequency, as not all the sensors have the same response properties. Although this addition is beneficial to the sampling process, testing should be done before grouping certain sensors on each device.

2.3.3 Deadband Transmission

In P. Hinterseer's work, a psychophysically motivated method was proposed by introducing "deadband transmission" [16], [15]. In the deadband transmission method, the output force is not updated unless the change in calculated force is above a certain threshold. This threshold, denoted as the *just noticeable difference* (JND), is a value measured by experiments, and anything below this threshold is deemed undetectable by humans. (Sensory threshold and JND are explained in Section 2.4.) For example, if the JND is 10% and the user is currently feeling a weight of 5 kg from the haptic device, the device will continue to output 5 kg even when the weight is increased to 5.2 kg. This is because the 0.2 kg difference is below the 10% threshold. When the weight is increased to 6 kg, however, the device has to update as the change is well above the threshold. An output graph will be similar to Figure 2.9.

The deadband used in this method is not restricted to force alone; velocity deadband is also used for making the decision for force transmission. This method is well-suited for teleoperation where communication between the master and the slave robot is critical. By creating force and velocity thresholds for transmission, the communication channel can be freed up while maintaining the same sensation for the users.

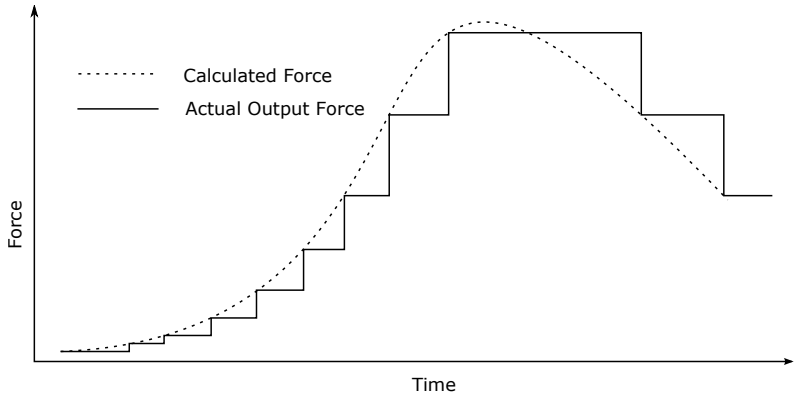

Figure 2.9: An example of force output from deadband transmission method.

2.4 Psychophysic Threshold and JND

Psychophysics is the study of sensation. It combines the *sensation* from psychology with *stimulus* from physics to develop methods to understand and quantify responses from sensory organs. Stimulus is the energy that is received by these organs to produce a sensation. The core study of psychophysics is to investigate *sensory thresholds*, which can be either the least amount of stimulus energy to produce a sensation, defined as the *absolute threshold*. The least amount of change in the stimulus energy, both increasing and decreasing, required to produce a stimulation is called the *just noticeable difference* (JND), or *difference threshold*. These thresholds differ from person to person, and may even change during the course of time, depending on the circumstances. Experiments usually consist of multiple subjects performing identical tasks repeatedly while the experimenter, or *observer*, supervises. The data collected are statistically analyzed to produce a conclusion.

Gescheider [11] presents a multitude of methods of constructing and operating these experiments and data analysis. There are many different approaches, with each characterized by different durations, sample sizes, and accuracies. Their main purpose is to give a statistical measurement to the human sensitivity threshold. The objective of this research is to find the minimum change in resolution, or JND, detectable by the human arm.

Therefore this section introduces some of the methods considered for achieving this goal.

2.4.1 Classical Psychophysical Theory

The methods presented in the following are classical measuring methods for sensory thresholds, specifically difference thresholds, although there are also variations for measuring absolute thresholds. Classical psychophysical methods involve an experimenter presenting a stimulus of known parameter (such as magnitude and frequency) for a subject to observe, and the subject responds with a description of his or her sensation. Since sensory thresholds change from time-to-time and person-to-person, an experiment usually contains sets of multiple trials given to multiple subjects with specified or randomized backgrounds.

According to *Weber's Law*[11], the change of stimulus intensity($\Delta\phi$) that can be distinguished from the standard stimulus (ϕ) is related with a constant fraction (c):

$$\Delta\phi = c\phi \text{ or } \Delta\phi/\phi = c \tag{2.2}$$

The linear relationship shown in (2.2) between starting intensity of the stimulus and JND-required intensity upholds when the starting intensity is large. However, when the intensity of the stimulus is low, experiments have shown that the constant c becomes larger [11]. A constant a is added to modify Weber's law to more closely model the trend.

$$\Delta\phi = c(\phi + a) \text{ or } \frac{\Delta\phi}{\phi + a} = c \tag{2.3}$$

Method of Constant Stimuli

In the method of constant stimuli, a reference, or *standard stimulus* (St), is paired with a *comparison stimulus* (Co) in each trial to be presented to the subject for comparison. The subject is expected to compare the two stimuli and state that whether the Co is "greater

than", "less than", or "equal to" the St. The level of intensity of Co is predetermined and evenly spread over a range of values where the lowest will always yield a "less than" response, and "greater than" for the highest. For example, if the St of an experiment to determine JND of hearing is 10 dB, then the Co can be 7, 8, 9, 10, 11, 12, and 13 dB. During the experiment, St-Co pairs are presented to the subject in a random order. A series may contain a minimum of 100 trials.

To find the JND, the percentage of "greater" response is plotted against the stimulus intensity in a psychometric graph. An s-shaped curve, or *ogive*, is then best-fitted on the graph. On this graph (e.g., see Figure 2.10), the value of comparison stimulus that yields 50% "greater" response is the *point of subjective equality* (PSE). The PSE represents the value which the subject perceives as equal to the standard stimulus. The differences between PSE and the 25% and 75% points of "greater" response are the lower and upper difference threshold, respectively. The difference threshold is usually calculated by taking the average of the lower and upper difference threshold. In the example, the stimulus values at 25%, 50%, and 75% are 1 dB, 2.4 dB, and 3.6 dB respectively. Therefore the upper and lower thresholds are 2.4 dB - 1 dB = 1.4 dB and 3.6 dB - 2.4 dB = 1.2 dB respectively, and the average of both threshold gives 1.3dB as the difference threshold.

Ideally, when comparing the standard and comparison stimuli, both stimuli are presented in the same space and time to get the most accurate discriminability. However, this will cause the sensation to overlap each other and become indiscriminable, completely opposite of the desired result. Therefore, the stimuli can only either exist in the same space at different times or vice versa. For example, images can be compared side-by-side and audio can be played in succession. However, when stimuli are presented in different locations, it is possible that the discrimination may be caused by the different receptor area instead of the difference in stimuli. This is referred to as *space error*. When the stimuli are presented in succession, it is found that subjects often find the second stimuli is greater

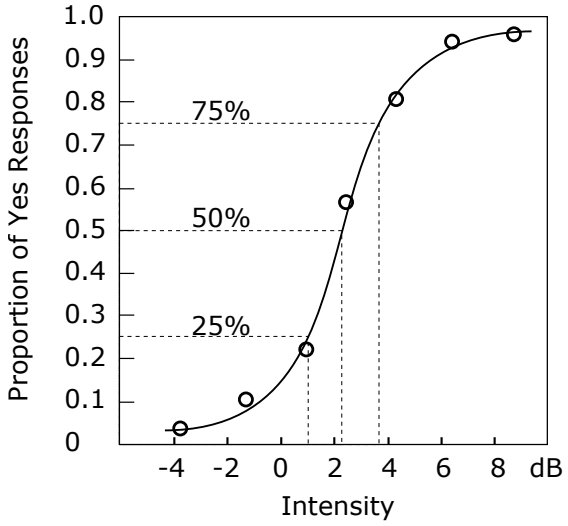

Figure 2.10: An example of a psychometric graph fitted with an ogive curve

than the first even when they are identical [11]. This is referred to as *time error* and it is believed to be caused by the fast-fading memory image of the first stimulus. Switching and randomizing the location or succession of the standard and comparison stimuli are the common methods of countering space and time errors, respectively.

Method of Limits

Like the method of constant stimuli, the method of limits is another frequently used procedure to measure sensory thresholds. It is claimed to be highly efficient with satisfactory results when certain errors are controlled to remain constant [11]. Unlike methods of constant stimuli, the method of limits does not require hundreds of trials in each series. Therefore it is a much faster technique.

To measure difference thresholds with method of limits, a standard stimulus is selected, and the size of incremental "steps" is determined prior to the experiment. While the presentation to the subject is similar to the method of constant stimuli where the standard stimulus is paired with a comparison stimulus to be presented to the subject, the progres-

sion of the comparison stimuli is not randomized like the former technique. The subject is expected to express the sensation as "less than", "equal to", or "greater than" the standard stimulus. The starting level of Co is much smaller than the St in an ascending series so that the subject will always respond initially with "less than". Similarly, the starting level is much larger than the reference in a descending series to always have a "greater than" response. In the ascending series, the comparison stimulus is increased by the predetermined step with each successive trial, and the series progresses until the subject response changes from "less than" to "equal to" to "greater than", and vice versa for descending series. The point where the sensation transition from "greater than" to "equal to" is referred to as the *upper limen* (L_u); the sensation transition from "less than" to "equal to" is referred to as the *lower limen* (L_l). The difference threshold is calculated by taking the average value of the upper limens and lower limens.

While performing the experiment, the subject runs into the risk of developing a habit of reporting the same response, and may either respond too early (*error of expectation*) or too late (*error of habituation*). The effects are minimal if these errors are of the same magnitude, but precautionary action must be taken. One method of reducing these errors is to randomize the starting level of the comparison stimulus. While the starting point still needs to be sufficiently larger or smaller than the standard stimulus, varying the level by a few steps for each series is often sufficient. Also, the method of preventing space and time errors mentioned in the method of constant stimuli should be used in this method as well.

In the example given in Table 2.1, it shows four sets of trials where two are ascending series and two are descending series. In the first ascending series, the trial starts with an stimulus intensity of -6 dB, a level where the subject is certain to give a "less than" (L) response. The intensity of the stimulus is increased until the subject feels the comparison stimulus is greater than the standard (G). Between the L and G transitions, there are a few stimulus levels where the subject cannot differentiate (E). Similarly, in the first descending

Stimulus intensity (dB)	A	D	A	D
8		G		
7		G		
6		G		G
5		G		G
4		G		G
3		G	G	G
2	G	E	E	E
1	E	E	E	E
0	E	L	E	L
-1	E		L	
-2	L		L	
-3	L			
-4	L			
-5	L			
-6	L			
L_u	1.5	2.5	2.5	2.5
L_l	-1.5	0.5	-0.5	0.5

Table 2.1: An example of four sets of trials for method of limits with ascending (A) and descending (D) series. The responses are "(G)reater", "(E)qual to" and "(L)ess than".

series, the trial starts with 8 dB, a level of intensity that the subject is certain to give a "greater" response, and then decreased until an "L" response is given. The subsequent A- and D-series vary their starting stimulus level to avoid the errors of expectation and habituation. The differential threshold of this example is the average of the limens of the four series: L_u =(1.5 dB + 2.5 dB + 2.5 dB + 2.5 dB)/4 = 2.25 dB, and L_l =(-1.5 dB + 0.5 dB - 0.5 dB + 0.5 dB)/4 = -0.25 dB, threshold = $(L_u + L_l)/2$ =1 dB.

2.4.2 Theory of Signal Detection and Application

The classical methods mentioned in Section 2.4.1, which produce sensitivity data purely in terms of electrical signals necessary to trigger a sensation, are insufficient. The Theory of Signal Detection (TSD)[11] more closely models human behaviour when a stimulus is detected with the concept of "noise". This noise may exist either in the background or generated by the sensory organs. Sensitivity is determined by whether or not the subject can discern the "signal" from the noise in an "observation". Therefore, in TSD, the trials either contain only noise (N) or a signal with noise (SN). An observation is the period of time when the subject may attempt to detect the signal within a trial. There may be multiple observations within a trial.

For TSD, the purpose is to transcribe the subject's performance into more than just sensitivity. Properties associated with sensitivity such as criteria and biases can also be measured and compared through the methods of TSD. A criterion is a threshold created by the subject for comparing signal levels. Anything the subject perceives that is over the criterion, either the signal or noise, is reported as a "yes", and anything below it is a "no". Response bias describes the subject's tendency to prefer one response over other ones, based on influences other than the signal intensity. The methods given in the following sections are some procedures developed using TSD.

Yes-No Procedure

In the yes-no procedure, the subject is given a large set of trials, usually in the hundreds, with a portion of the trials containing a signal (SN) while the rest do not (N). The subject's role is to respond with "yes" or "no" to indicate whether a signal is detected or not, respectively. From the subject's point of view, this is similar to the method of constant stimuli. An experiment shall contain a number of trial series, with each series having a different percentage of SN trials. For example, an experiment may contain five sets of trials with 10%, 30%, 50%, 70%, and 90% of the trials contain a signal. At the beginning of each series, the subject is informed of the percentage of SN in that series. Indicators or cues are used to indicate the observational period. For example, a signal light may turn on when the subject is required to make an observation.

The response from the subject for each probability is split into percentages of hit [p(yes|Y)], miss [p(no|Y)], correct rejection [p(no|N)], and false alarms [p(yes|N)]. The sensitivity of the subject can be related to the percentages of hits and false alarms. By plotting the relationship between hits and false alarms, a *receiver-operating characteristic curve* (ROC curve) can be obtained. An example of a ROC curve is shown in Figure 2.11a. The significance of a ROC curve is to approximate detectability of the subject, which is shown in Figure 5.9 of Gescheider [11]. There are also other methods for comparing sensitivities. For example, in the event of a single experimental set and a ROC curve can not be plotted, Pollack and Norman proposed Equation 2.4 for calculating sensitivity, A', [11].

$$A' = \frac{1}{2} + \frac{[p(\text{hits}) - p(\text{false alarms})][1 + p(\text{hits}) - p(\text{false alarms})]}{[4p(\text{hits})][1 - p(\text{false alarms})]} \tag{2.4}$$

An example of a yes-no procedure involving five sets of trials is given in Table 2.2. The intensity of the SN is constant, but the percentage of SN contained in the set is varied.

Signal Portion	Hit	Miss	Correct Rejection	False Alarm
	[p(yes|Y)]	[p(no|Y)]	[p(no|N)]	[p(yes|N)]
10%	0.26	0.74	0.93	0.07
30%	0.45	0.55	0.81	0.19
50%	0.71	0.29	0.64	0.36
70%	0.78	0.22	0.52	0.48
90%	0.93	0.07	0.30	0.70

Table 2.2: Example results of the Yes-No method

Using the plot in Figure 2.11a, the detectability for this stimulus is estimated to be around 1.0 when matched to Figure 2.11b.

Forced Choice Procedure

A disadvantage of using the yes-no procedure when applying to haptic measurements is that the required number of trials is too large, which is usually in the hundreds. The forced-choice method, similar to the method of limits, can obtain the most accurate sensitivity data within the shortest period of experimental time.

In the forced-choice procedure, the subject is presented with a number of stimuli in a trial, but only one of them is the comparison stimulus while the rest are the standard stimuli. This comparison stimulus is randomly placed in the group, and the subject is expected to pick it out. The resulting data are simpler than the yes-no procedure as there are only "hits" and "misses". This method yields a better result than the yes-no procedure due to the constant comparison between N and SN stimuli, thus reducing the chance of "guessing" from the subject. The accuracy increases as the stimulus group increases. For example, the result from a four-alternative forced choice (stimulus is contained in four possible choices)(4AFC) is more accurate than a 2AFC (stimulus is contained in two

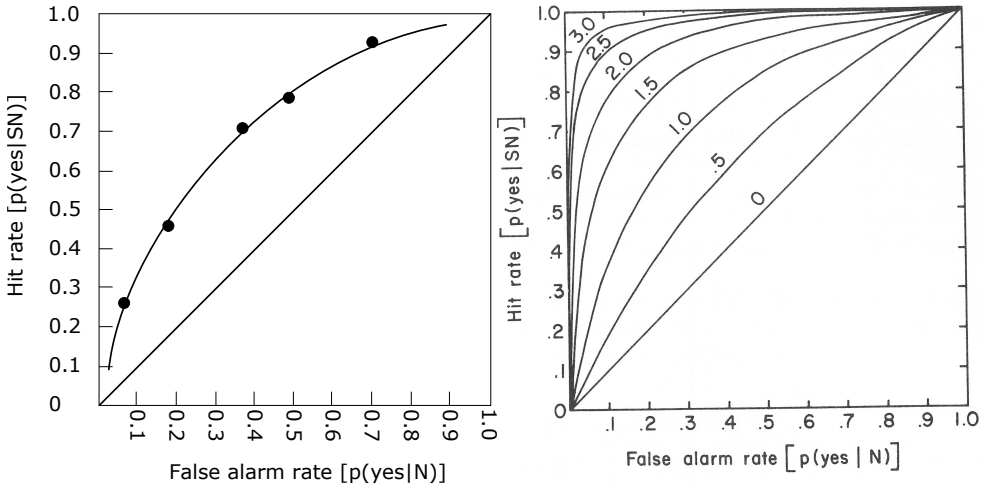

(a) Example plot of Yes-No method (b) Family of detectability plots [11]

Figure 2.11: Example plot of the Yes-No method

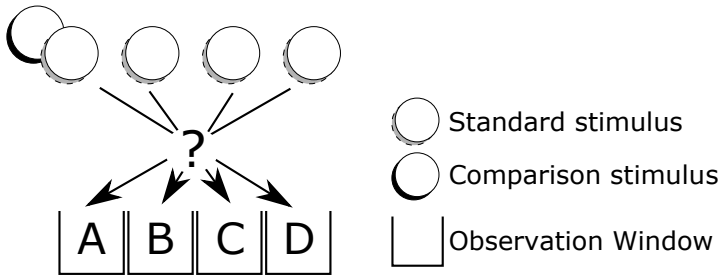

Figure 2.12: An example of a single trial in a 4AFC forced-choice method

possible choices) as the chance of guessing correct in a one-out-of-four situation is much lower than one-out-of-two.

A single trial of a 4AFC example is illustrated in Figure 2.12. The comparison stimulus with certain stimulus intensity is paired with the standard stimulus of this particular set, and then randomly placed in one of the four observation windows with three other containing single standard stimuli. The subject, after being presented with all four observation windows, is expected to pick the one window that contains the comparison stimulus.

Forced Choice Tracking

The forced-choice-tracking method (FCT) is a modification of the forced-choice method that adds an adaptive characteristic to the original method. FCT is designed to measure the sensory threshold where the subject can correctly detect at a fixed percentage of hits, which means the percentage of correct, $p(c)$, is fixed. The intensity of the successive comparison stimuli is adjusted according to the current record of the subject's hits and misses, usually by a fixed step. A FCT experiment begins with a comparison stimulus intensity level that is detectable at all times, and, with every miss the subject makes, the intensity increases by a predetermined step[7]. For every hit, not necessarily consecutive, the intensity of the stimulus decreases. For example, to achieve a $p(c)$ rate of .75, every three correct choices the subject makes (again, they *do not* have to be consecutive), the intensity is decreased. By the end of the experiment, the subject will have achieved the target $p(c)$ by varying the stimuli around the threshold. The starting stimulus level, incremental step, and experiment length are also optimally chosen to achieve this target.

An example of a FCT measurement is given in Figure 2.13. The adjustment of the intensity is determined by the performance of the subject. An incorrect choice (I) decreases the intensity while a number of correct ones (C) may increase it. The threshold is taken as the average of the results from trial 6 to 15, which is approximately 4.5 dB.

The FCT is an adaptive measuring method, and, according to Macmillan and Creelman [11], an adaptive experiment must be defined by answering these four questions:

1. "What results should lead to a decision to end testing at the current level and shift to a new one?"

2. "When the stimulus level is to be changed, to what level should it be changed?

[7]The *intensity level* mentioned in this section is the difference between the comparison stimuli and the standard stimuli, and not the absolute value of the intensity level.

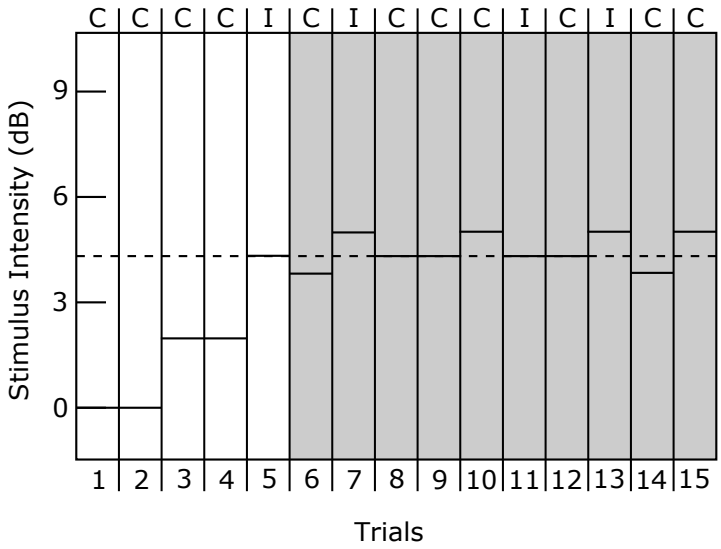

Figure 2.13: Example of a forced-choice tracking measurement

3. "When does an experimental run end?"

4. "How should an estimate of threshold be calculated?"

In FCT, (1) the current intensity level for the comparison stimulus shifts to a new one when the subject either makes a "miss" or a predetermined number (not necessary consecutive) of "hits", (2) the size of the change is predetermined, (3) the experiment ends when sufficient data produce a predetermined $p(c)$, and (4) the threshold is calculated by taking an average of the data that have reached a stable tracking threshold.

The FCT is the most suitable method for the purpose of measuring muscular sensitivity out of all the psychophysical measurements mentioned in this section. One aspect of the experiment to be wary about is the length of each experiment, as any prolonged physical activity may affect muscular sensitivity [41],[6],[3]. Due to this, the measurement method has to be short in duration to avoid bias caused by fatigue. The lowered requirement for the number of samples in FCT can minimize the effect of fatigue while retaining accurate results.

2.5 Analysis of Variance

When an experiment is performed by observing the behaviours of subjects in different control groups, the resulting data is usually spread across a range of possible outcomes. The common approach to obtain a presentable result is to take the mean value of all the data within the groups, and also to calculate the standard error to indicate the significance of the results. When there are one or more control variables involved in the experiment, the experimenter has to determine whether the results are affected by the variables or completely due to chance. To determine how significantly the observation data collected are affected by the associated control variables, the *analysis of variance* technique is applied.

Analysis of variance, commonly referred to by the acronym ANOVA, was developed by R. A. Fisher[36] to test observational data against controlled experiment variables. Since test results are often affected by noise and/or other biases, ANOVA can be used as a *test of significance* to conclude the relationship between test variables and the observations. If there are two or more independent sets of variables, a two-way or multi-way ANOVA can also analyze the significance of the interaction between those variables.

2.5.1 Two-Way ANOVA for Repeated Measures

A *repeated measures* experiment is one that has all its subjects perform all the experimental sets. Therefore, every subject has experienced each combination of control variables exactly one time. In this research, all the experiments are designed to have two control variables (one being the movement speed, and surface property being the other) and all subjects within a group have to perform all sets of tests within the experiment. The most appropriate analysis for the experiments performed in this research is the two-way ANOVA for repeated measures.

In a two-way ANOVA, there are two independent variables, A and B, and subjects R.

Subject	A_1			A_2		
	B_1	B_2	B_3	B_1	B_2	B_3
R_1	S_{111}	S_{112}	S_{113}	S_{121}	S_{122}	S_{123}
R_2	S_{211}	S_{212}	S_{213}	S_{221}	S_{222}	S_{223}
			$\vdots$			
R_n	S_{n11}	S_{n12}	S_{n13}	S_{n21}	S_{n22}	S_{n23}

Table 2.3: Example data for repeated measures experiment.

Source	Type III SS	DF	Mean Sq.	F	Prob $>F$
A	7.4	2	3.7	6.7	0.0054
Error(A)	12	22	0.56		
B	0.58	1	0.58	0.91	0.36
Error(B)	7.0	11	0.63		
$A * B$	2.7	2	1.3	2.3	0.12
Error($A * B$)	13	22	0.58		

Table 2.4: Example of two-way ANOVA for repeated measures

Each variable can contain two or more levels, such as A_1, A_2 and B_1, B_2, B_3. For each R, the data values S from the experiment are obtained by a combination of the independent variables, e.g., A_1B_1 or A_2B_3. Running an ANOVA analysis on the results can determine how A and/or B affects the data. In an ANOVA table (see Figure 2.4), there are five values associated with each variable and each interaction ($A*B$), degree of freedom (DF), mean square (MS), sum of squares (SS), F-value (F), and p-value (p). The DF, MS, and SS values can also be calculated for the random error associated with each variable and interaction, which are referred to as Error(A) and Error($A * B$).

Degree of freedom is the number of levels minus one ($n_A - 1$) for the variables and

number of subjects minus one and multiplied by the DF of the associated variable ($(n_R - 1)(n_A - 1)$) for error. For example, if 12 subjects are observed ($n_R = 12$)in the experiment involving the A and B variables mentioned above, then the DF of A, B, Error(A), and Error(B) would be 1, 2, 11, and 22 respectively. The sum of squares commonly used by ANOVA is a Type III SS, which is the marginal sum of squares. This is preferred over the other types because a Type III SS is unaffected by the frequency of observations, which means the number of observations does not have to be balanced. The mean square of a variable estimates the variation of all observations associated with the variable and its levels, and the MS of the error estimates the variation of all observations only. The value of MS is simply the SS value divided by the corresponding DF.

The F-value is the ratio between the MS of a variable and the MS of its error, given by Equation 2.5. The significance of the F-value is to determine whether the difference in the means resulting from the variables is caused by random noise. A large F-value (depending on the corresponding DF) may mean significant correlation between the variables and observations.

$$F = \frac{\text{Mean Square of } A}{\text{Mean Square of Error}(A)} \tag{2.5}$$

The p-value is the probability of finding a difference of means as large as or larger than the values found in the experiment. If the probability p is less than 5%, then the effect of the variable on the results is said to be "significant"; if p is less than 1%, then it is "highly significant". In the example shown in Figure 2.4, control variable A has 3 levels, B has 2 levels, and there are 12 subjects. Variable A, with a p-value less than 1%, is rated as "highly significant" for the trend observed in the data, whereas variable B and their interaction ($A * B$) are not. The format to present the results of ANOVA table is commonly written as F(DF(A), DF(Error(A))) = F(A), and p = p(A). In the example given, it will be $F(2, 22) = 6.7$, and $p = 0.0054$.

Chapter 3

Experimental Design

The objective of the experimental setup is to provide a virtual environment with haptic models for the test subject to feel, and to collect speed-sensitive sensory responses from him or her. Along with a human operator, the setup guides the subject through different sets of experiments and assists in maintaining a constant movement speed of his or her arm. The setup also provides haptic surfaces with different properties, and switches between them when required to mimic a multiresolution model. The psychophysical measurement method, forced-choice-tracking (FCT), is implemented in the setup to measure the sensory thresholds of each subject. The force applied by the subject during the experiment is also collected for reference.

3.1 Overview

The experimental setup consists of a desktop workstation with a haptic device. The subject is to be seated in an up-right position in front of the workstation while performing certain haptics-related tasks and responding to specific questions. A monitor is available to the subject for providing visual cues. The experimenter, who sits beside the subject

for supervision purposes, will use the keyboard of the workstation to control the experiment. There are two main parts to the experimental procedure, the training phase and the experimental phase. The training makes sure all the subjects can maintain their arms' movement speed with the aid of the visual display and understand the presentation of the standard and comparison surfaces. The experimental phase consists of six tests, and each test asks the subjects to differentiate two surfaces with slight differences. The sensitivity data for each subject are collected as he or she progresses through the tests.

The software of this design is written in C++ with the OpenHaptics™ V3.0 library from SensAble Technologies to interface with the haptic device and the OpenGL® library for graphics rendering. On top of the subjects' responses, the software also records the magnitude of the haptic device's force output at a rate of 10 Hz for the duration of the test.

3.2 Kinesthetic Feedback Devices

Because haptic devices are still fairly uncommon as a user interface, no industry standard has been set. Research related to haptic feedback either uses a readily available device on the market or resorts to building a proprietary prototype. The main advantage of having a proprietary haptic device is that its dynamics should be well-known to the researcher. However, building a custom device is time-consuming, and the data it produces may be device-specific. Having device-specific data can make future research less reproducible without the exact same device. Using a readily available device on the market eliminates this problem because factory standards ensure that each unit's specifications are within a tolerable range of one another.

There are three readily available haptic devices for experimental design: the Phantom Omni and the Phantom Desktop models from SensAble, and the Falcon from Novint. All

Device	PHANToM Omni	PHANToM Desktop	Falcon
DOF	6	6	3
Max Force (N)	3.3[1]	7.9[1]	8.9
Continuous Force (N)	0.88	1.75	8.9
Backdrive Friction (N)	< 0.26	< 0.06	N/A
Workspace (mm)	160 W 120 H 70 D	160 W 120 H 120 D	101.6 W 101.6 H 101.6 D
Resolution(dpi)	> 450	> 1100	> 400

Table 3.1: Technical specifications of haptic devices, [28], [20], [19]

are force-feedback haptic devices as introduced in Chapter 2. The properties of all three devices are compared in Table 3.1.

When choosing the most suitable device out of the three, the follow criteria are considered.

1. *Force output.* This experiment is designed for the subject to maintain constant contacts with a stiff, non-deformable model, therefore, if the force output is not sufficiently high, the subject may not feel the intended tactile feedback.

2. *Dynamics of device.* Without the exact mechanical design of the device for dynamics modeling, the chosen device should at least minimize mechanical nonlinearities, such as low friction.

[1]This is the maximum exertable force at nominal (orthogonal arms) position [20], [19].

Overall, the Desktop is a superior unit over the Omni, in both the above criteria, higher sensitivity, and lower friction. These characteristics make a stiff model actually feel "stiff" with the Desktop, but rather soft when using the Omni. When compared to the Falcon, the Desktop is better in terms of ergonomics and workspace, even though the Falcon has a higher force output. Ergonomics is an important factor as the design needs to minimize awkwardness when using the haptic device. The pilot study subjects have all intuitively held the stylus interface on the Desktop as a pen, but each individual has a slightly different way of holding the ball-shaped interface on the Falcon. As for the workspace, having a larger workspace reduces the possibility of the subject hitting the mechanical limits of the device during usage and affecting the force sensitivity. The PHANToM Desktop was ultimately chosen for the experimental setup.

3.3 Graphical Display

One of the most integral parts of the design of the experimental setup is the graphical display. While this research is focused on the sense of touch, the right amount of visual information can provide a sense of immersion for the subject in the new environment. However, if poorly designed, the interface may increase the *extraneous cognitive load* and prove to be more of a distraction[1]. The latter may result in biased data. The amount of information displayed for the subject must be carefully considered.

When designing the interface, the main concerns are what type of information the subject sees and how the information is presented. For example, first and foremost, the subject needs to know his or her hand's position relative to the other virtual objects in the environment, such as the surface model. Therefore the presence of a cursor is necessary.

[1]Extraneous cognitive load is the unnecessary information within instructional material, as described by Chandler and Sweller, [4].

This section goes through the design considerations when creating each object that the subject sees on the monitor.

3.3.1 Graphical User Interface

After a few pilot studies, the final design of the graphical interface consists of the following objects: a three-sided wall, a cursor/speed indicator, and a defined surface. The wall gives the subject a sense of boundary and defines the size of the workspace. During the test, the subject is instructed to restrict his or hers hand movement to within the walls. The walls serve as visual cues, and since the walls are created as haptic surfaces with the highest stiffness setting, they provide force feedback as well. Any contact with the wall is forbidden since there will be an undesired force effect on the subject.

The defined surface is the graphical representation of the haptic surface. It is placed at the bottom half of the screen, and it can be enabled and disabled, depending on the requirements. The cursor can either be cylindrical-shaped, which is explained in section 3.3.2, or conic. Any other shape (except for a dot) for the cursor may be counter-intuitive since the haptic device only provides a point contact with the haptic models. The conic cursor is a generic cursor that follows the motion and orientation of the stylus interface of the haptic device.

3.3.2 Speed Indicator

The most challenging part of this design is to assist the subject in maintaining his or her arm at a constant speed as it moved across the surface. There were a few options considered during the design process, including, but not limited to, assisted movement, a numerical display, and speed indicators.

For assisted movement, the plan was to move the end-effector on the haptic device by a position controller. The subject only had to hold on to the device and apply forces in the vertical direction. This method would have ensured a uniform speed for all subjects. However, the induced sensation on the subject's arm was deemed "unnatural". Another option was to introduce an oscillating "target" which the subject had to follow with the cursor. This target was comprised of two vertical bars which represented a tolerance range of position (shown in Figure 3.1). The bars would move at the designated speed, oscillating left and right. The subject maintained the speed by keeping the cursor between the target. This proposal was scrapped because, during the pilot study phase, subjects were complaining that the moving target was too distracting and hard to follow. A numerical display of the speed was also considered, but it was also removed as it was deemed too distracting, for the subject had to focus on both the number and the cursor.

After positive feedback from pilot study subjects, the method of maintaining constant speed of the subject's arm was to use three colours to inform the subject whether his or her speed was too slow (blue), too fast (red), or within the tolerable range (white). This indicator was combined with the cursor. The subject only had to focus on a single object on the screen.(Figure 3.2 The speed readout from the haptic device was averaged over seven samples at 60 Hz to reduce flickering of the cursor due to the instantaneous increase or decrease of speeds[2].

3.4 Experimental Procedure

As mentioned at the beginning of this chapter, the experimental setup consisted of a desk-top workstation with a haptic device. For each experiment, there was a volunteer test subject accompanied by the experimenter. The experimenter first introduced the purpose

[2]The number of samples for averaging was determined during the pilot study phase.

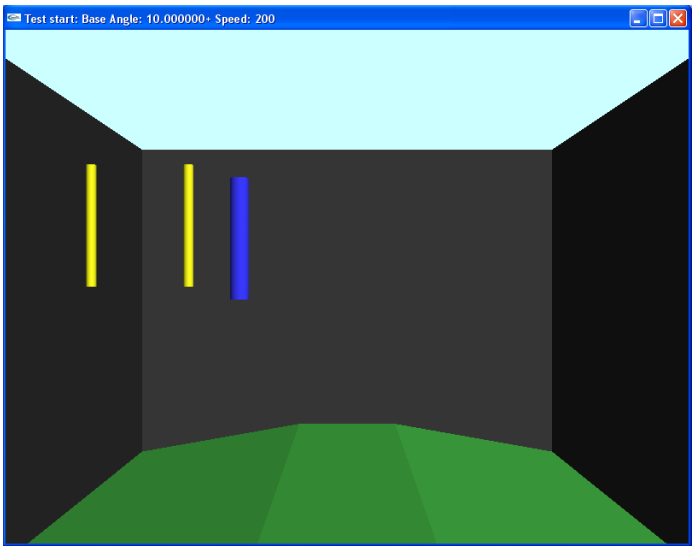

Figure 3.1: Twin-bar target for speed control. The cursor (bar on right) is always suppose to be in between the two bars on the left.

of the experiment, and then guided the subject through the training phase for familiarization with haptic devices before going onto the experimental phase for data collection.

3.4.1 Subject Training

One of the requirements in the design of the experiment is to minimize the time that the subject should spend on getting accustomed to the experimental setup. Since this is a test of force sensitivity while the subject moves his or her arm and maintains contact with a haptic surface, a prolonged training period may generate stress in the arm's muscles and may affect the results. To quickly let the subject associate the haptic surface with a geometric shape and to accommodate the subject's possible lack of experience with a haptic device, a visual representation of the haptic surface is necessary.

There are two parts of the training phase - the first one is familiarization with haptic devices and the second one is being able to recognize visual cues for maintaining constant

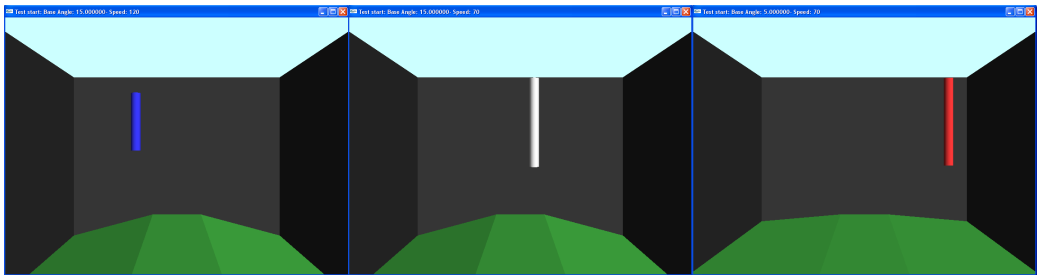

(a) Too slow. (b) Within range (c) Too fast.

Figure 3.2: Three colours of cursor for speed indication

speed and pressure during the experimental phase. In the first part, after the subject sits down in the proper position in front of the workstation while holding the haptic device in his or her dominant hand, the subject is presented with a mesh surface model. The subject is encouraged to freely explore the virtual environment with the haptic device. At this point, the cursor is represented by the generic cone mentioned in Section 3.3.1. This part lets the subject quickly associate the haptic interface with the graphic interface.

The second part is the more critical part. (This is also the setup phase of the test program, as the experimenter can set the test parameters.) In this part, the cylindrical cursor with speed indication replaces the generic cone. The cursor only follows the subject's position in the x-direction as it stays at the same height and depth. The length of the cursor is an indicator of the magnitude of the normal force exerted by the haptic device. The operator can check whether the subject has made contact with the surface before starting the test. A geometric surface is also presented as reference, although the cursor never appears to be in contact with the surface. The subject is instructed to move the cursor left-and-right at such speed that the cursor becomes white. While maintaining this motion, the subject can only use his or her elbow and minimize wrist motion. No wrist strap is provided to constrict the subject's arm, but a gel pad is provided as elbow support. The subject is also required to maintain contact with the geometric surface while in motion.

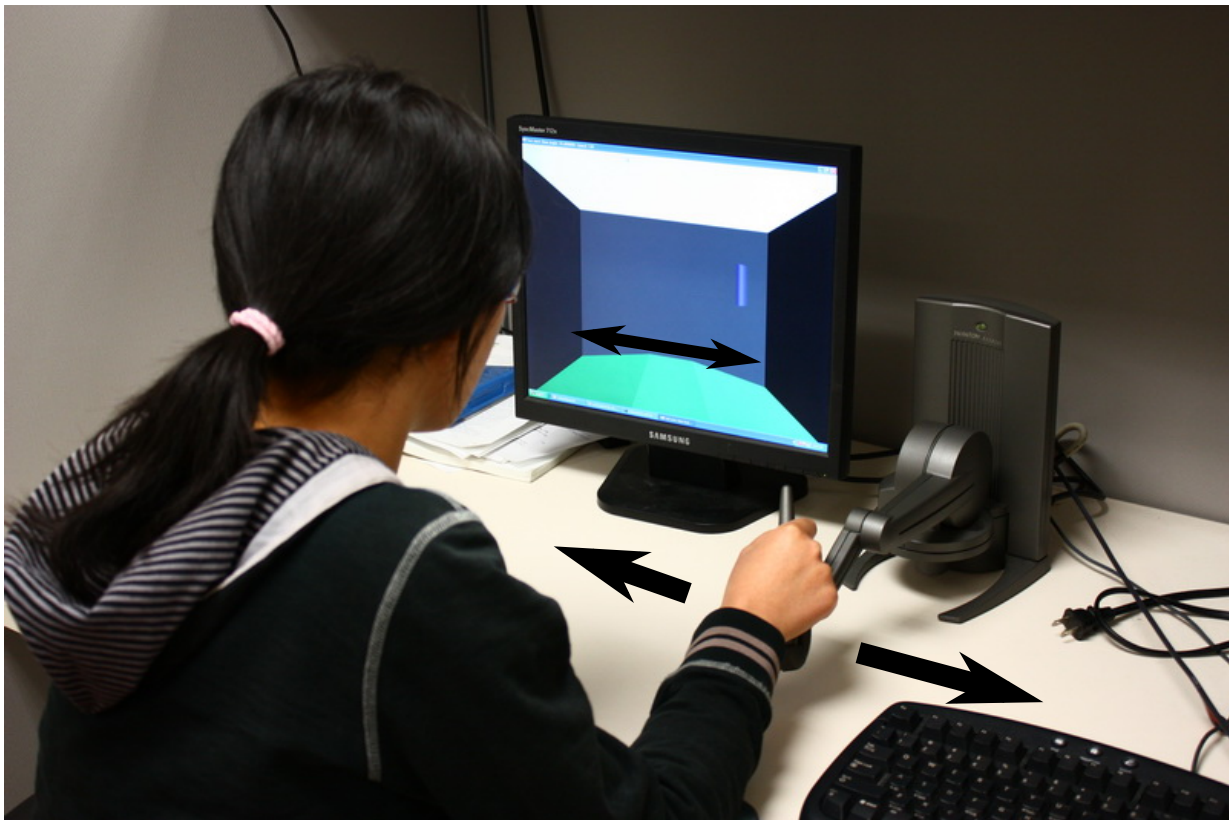

Figure 3.3: Experimental setup with subject's hand motion illustrated

Once the experimenter has assessed that the subject can maintain the constant required speed with minimal effort, the experimental phase may begin.

3.4.2 Experimental Phase

For each experiment, a type of haptic surface is chosen as the *standard surface* (SS), and parameters of each surface are chosen for generating *comparison surfaces* (CS) for JND measurement. For example, the first experiment (Chapter 4) measures the force JND for changes in resolution, so the comparison surface shares all the same properties as the standard surface except for its resolution. Two standard stimuli are created for each experiment by varying one of the properties.

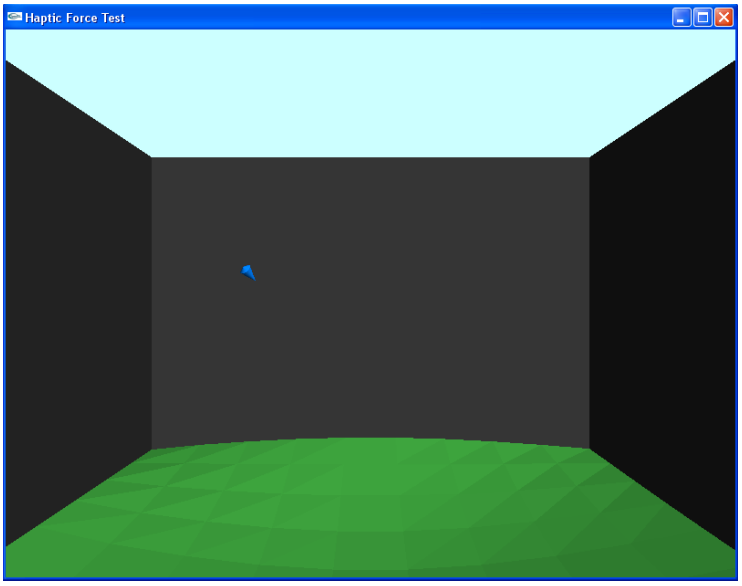

(a) Introduction to haptics

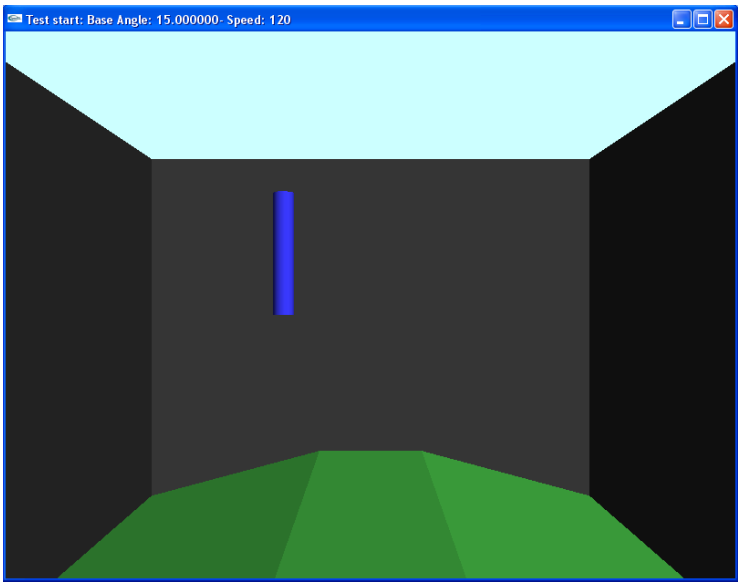

(b) Speed training

Figure 3.4: Different interfaces for training subjects

Three speeds were chosen as benchmarks - 70 mm/s, 120 mm/s, and 200 mm/s, denoted as *low speed* (LS), *medium speed* (MS), and *high speed* (HS) respectively. The lowest speed was chosen as a low, yet comfortable speed through the pilot studies. These three speeds were used for both experiments for standardized comparison. The two standard surfaces from each experiment were paired with each of the subject's hand's speeds to form six experimental sets.

For the method to measure JND, this research implemented the forced-choice-tracking procedure (FCT), which was the adaptive variation of forced-choice procedure. FCT has the advantage of requiring the least number of trials and minimizing possible bias. As mentioned in Section 2.4.2, the FCT requires a *standard stimulus* to be compared with multiple *comparison stimuli*. In this research, the standard stimulus and comparison stimulus were the sensations generated by the standard surface and the change of the two surfaces, respectively, when the subject was moving across the surface. The threshold of the JND was achieved when the subject could not discern the change from absolutely no change at all (SS-SS). The percentage of correctness was set to 0.75 for the FCT threshold, i.e., the subject could only correctly identify the SS-CS change three out of four times.

After the pilot study, the effective number of trials per experimental set was determined to be 30, and mandatory breaks were given between each sets. The surface-speed pairs were also given in random order for each participant to equally distribute the effect of fatigue in all experiments.

For each subject, he or she is presented with:

- Six sets of tests, for two standard surfaces and three different speeds.
- Each set contains thirty trials, each with a corresponding comparison surface.
- Each trial contains two cases: case A and case B. Only one of the cases from each trial contains the comparison surface. The other one does not change. This is randomly

generated by the test.

To prevent the subject responding before the comparison surface has been presented, a visual cue is given. The colour of the wall element in the virtual scene serves as an indicator to the subject as to the moment the subject should expect the occurrence of the change. Under normal operation, the wall is shaded with dark-gray. When a test case is presented in a trial, the colour of the wall is switched to light-gray and this is maintained for two seconds. The standard surface is always present during the two-second period. After two seconds, the colour of the wall changes back to dark-gray, which is an indication to the subject that, should the surface be changed to the comparison surface, this is the moment of change. If the change does occur in this test case, then this is maintained for one second before switching back to standard surface. The colour of the wall does not change in the second switch. This procedure for each trial is illustrated in the timing diagram in Figure 3.5, where *visual cue* represents the colour of the wall during each period.

For each set of the test, the procedure is of the following:

1. The subject accelerates to the targeted speed.
2. The operator makes sure that the subject is moving within the correct range of speed and is in contact with the surface before proceeding.
3. The operator presents case A.
4. The operator checks the force-recording process has finished, then presents case B.
5. The operator waits for the subject's response, enters the corresponding key, then proceeds with the next trial.
6. The operator repeats this process for the entire set of the experiment for the required number of trials. Breaks can be offered at any time of the trial by the subject's request.

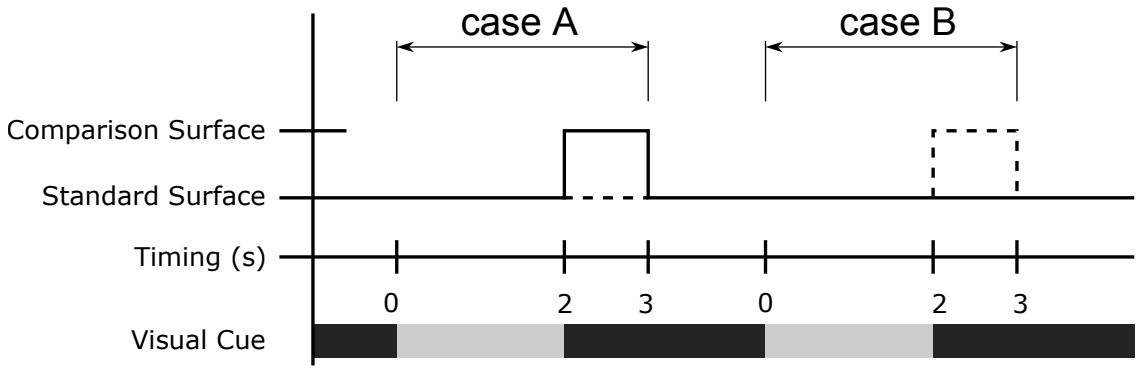

Figure 3.5: The timing of the test procedure.

After both case A and B from one trial are presented to the subject, the subject is required to respond with the case where a change is felt. Uncertainty is not allowed. The subject is told beforehand that, in the case of uncertainty, an instinctive guess should be made. This makes "case A" and "case B" the only possible choices for a response. The responses from the subjects are gathered in a text file to be analyzed in a separate process.

Chapter 4

Experiment One: JND of Resolution

The objective of this experiment is to determine the just noticeable difference (JND) with changes of small surface details with respect to the user's movement speed. The subject is asked to feel a haptic surface with a constant radius of curvature, i.e. a cylindrical curve, at three different speeds, and the resolution of the surface is changed during the tests. This experiment determines the threshold where the subject cannot distinguish the two surfaces with identical curvatures but different surface resolution at certain speeds.

4.1 Hypothesis

The hypothesis tested in this experiment is stated as follows:

> H_1: The JND of human perception for haptic surface resolution increases when the movement speed of the user's hand increases in a haptic environment with multiresolution models.

This hypothesis is motivated by the velocity-driven multiresolution haptic compression technique developed by Kolčárek[23], where the haptic model resolution is inversely pro-

portional to user's movement speed while in contact with the model.

4.2 Method

Using the virtual environment described in Chapter 3, two haptic surfaces are selected to be the standard surfaces used in the Forced-Choice Tracking (FCT) measurement. Both surfaces have the highest stiffness setting allowed by the haptic device, the PHANToM Desktop. The subjects are trained to feel the surfaces at the three average speeds specified in Section 3.4.2: 70 mm/s (LS), 120 mm/s (MS), and 200 mm/s (HS). The properties of the surface are defined in Section 4.2.1.

4.2.1 Surface Definition

The two standard surfaces are cylindrical curves with radii, R, of 86.8mm (Surface-A) and 148mm (Surface-B), with Surface-B illustrated in Figure 4.1. Each surface is its own experimental set. The reason for choosing a curved surface is because it has a simple geometry, yet it feels different depending on the resolution of the surface. For instance, a high-resolution model may feel "smooth" to the touch, while a low-resolution one may feel "bumpy" with the more distinct edges and individual faces. This experiment measures the transition point between the points where a subject cannot distinguish between a surface of high-resolution and one with lower resolution.

The standard surface model uses a resolution, n, of 30. The "resolution" of the surface is defined to be the number of divisions for each half of the surface in this experiment. The number of vertices for each curve is $2 \cdot n + 2$ (e.g., with a resolution of 30, the standard surface has 62 vertices on the curve). Instead of having each vertex lying on the surface, the positions of the vertices are defined by the tangential line between each vertex, as

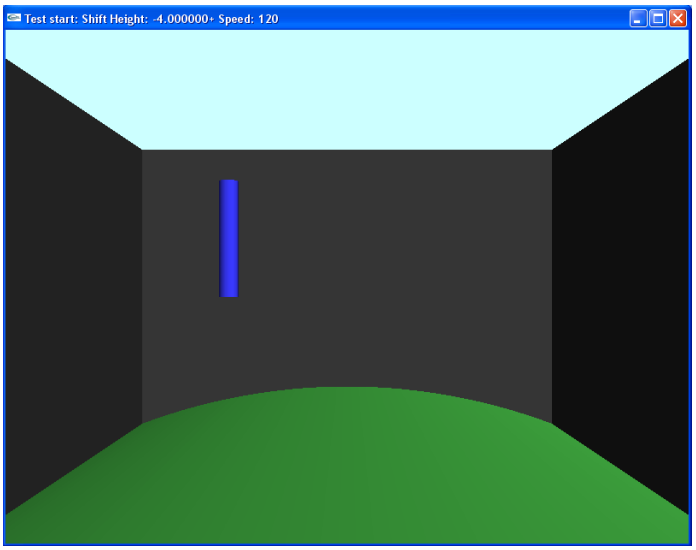

Figure 4.1: The screenshot showing the cylindrical haptic surface with resolution of 30 in the experimental phase.

shown in Figure 4.2. By defining the surface in this method, the maximum height of the surface does not change with the resolution.

The length of each of those flat faces, (x), and the angle (θ) between each of them are defined by Figure 4.2. Equations 4.1, 4.2 and 4.3 give the calculations to find the values of φ, θ, and x on the figure respectively. For all of the surfaces used in the experiment, L is 106 mm. There are two different values for R: 86.8 mm (Surface-A) and 148 mm (Surface-B). and their values for both surfaces used in experiment one are given in the Table B.1 in Appendix B. The rows of Table B.1 are arranged by the difference in resolution relative to the resolution of the standard surface, $n = 30$, for which the values are in the first row.

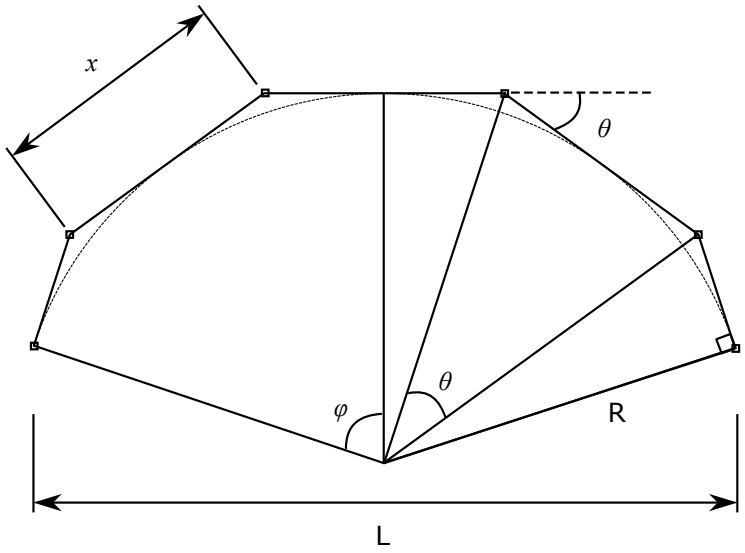

Figure 4.2: Definitions of x and θ

$$\varphi_R = \text{asin}\left(\frac{L}{2R}\right) \tag{4.1}$$

$$\theta_{R,n} = \frac{\varphi_R}{n} \tag{4.2}$$

$$\begin{aligned} x_{R,n} &= 2R \cdot \tan(\theta_{R,n}) \\ &= 2R \cdot \tan\left(\frac{\varphi_R}{n}\right) \end{aligned} \tag{4.3}$$

The percentage differences for all the x and θ values are calculated against the values associated with the standard surface, which is $n = 30$. The θ values are calculated by Equations 4.4. The calculation in Equation 4.5, the calculation for percentage difference of x-values, shows that it is the same as Equation 4.4 when $n \geq 10$ since the tangent of a small angle is approximately the value of the angle in radians.

$$
\begin{aligned}
\%\text{diff} &= \frac{\theta_{R,n} - \theta_{R,30}}{\theta_{R,30}} \\
&= \frac{\frac{\varphi_R}{n} - \frac{\varphi_R}{30}}{\frac{\varphi_R}{30}} \\
&= \frac{30 - n}{n}
\end{aligned} \tag{4.4}
$$

$$
\begin{aligned}
\%\text{diff} &= \frac{x_{R,n} - x_{R,30}}{x_{R,30}} \\
&= \frac{2R \cdot \tan\left(\frac{\varphi_R}{n}\right) - 2R \cdot \tan\left(\frac{\varphi_R}{30}\right)}{2R \cdot \tan\left(\frac{\varphi_R}{30}\right)} \\
&\cong \frac{\frac{\varphi_R}{n} - \frac{\varphi_R}{30}}{\frac{\varphi_R}{30}} \text{ for } n = 10 \rightarrow 30 \\
&= \frac{30 - n}{n}
\end{aligned} \tag{4.5}
$$

The comparison surfaces in each experimental set are created by changing the resolution of their respective standard Surface-A and Surface-B models. The initial comparison surfaces have $n = 2$ for the surface to generate a significant noticeable difference at the beginning of each experiment. To ensure that the subject can experience the difference in the first few trials and then reach the sensory threshold before the end of the experiment, the design has taken a non-linear approach to vary the resolution difference.

By using the Equation 4.6, the difference between the standard surface and the comparison surface resolutions is large enough in the first few trials to approach the threshold, and it gets finer in the last few trials for a more precise threshold value. (The criteria for change in FCT is either the subject makes an incorrect choice or three correct choices.) The com-

parison surface's resolution is never higher than the standard surface's, (i.e., $2 \leq n \leq 30$). Equation 4.6 is found by trial-and-error during the pilot study phase.

$$\text{Resolution Change} = 2 \cdot \left(\frac{\text{\# Trial Left}}{12} \right)^2 + 1 \tag{4.6}$$

4.3 Participants

The participants were selected randomly from the graduate student body of University of Waterloo. There were approximately 40% females, and 90% of the total were from the Faculty of Engineering. Only one of the subjects was left-hand dominant, while all others are right-hand dominant. The age of the subjects ranged from 23 to 30 years old. Each of the subjects had various degrees of familiarity with haptic devices, which ranged from "none at all" to "used them in research". All of them were familiar with a 3D virtual environment. The University of Waterloo office of research approved the experiment as Research Involving Human Participants (ORE #16157). The experiment was conducted in accordance with the University of Waterloo ethical guidelines. Signed consent letters were obtained from all participants prior to the experiments.

4.4 Results

The response data collected from the 12 subjects are in resolution, n. The calculated threshold values for each subject are given in Table A.1 in Appendix A. A sample FCT measurement from the experimental set Surface-A + HS is given in Figure 4.3. The results are taken as the average of the last 15 trials of each test case, where the JND is the average percentage change after the conversion. The statistical results from all subjects are shown in Table 4.1, and a graphical representation of the data is shown in Figure 4.4a. The

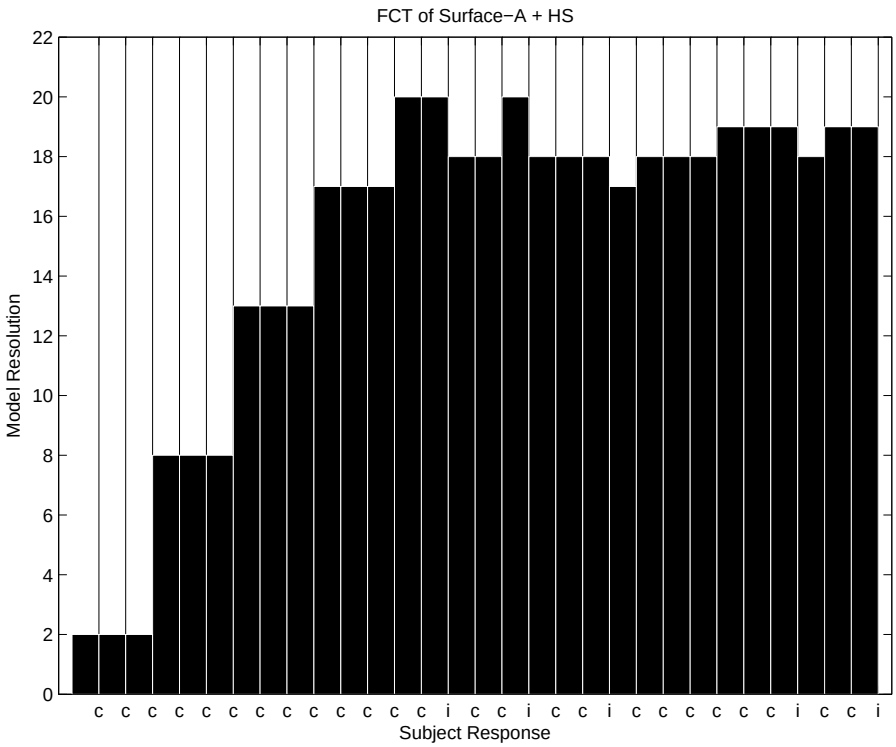

Figure 4.3: A sample FCT plot for Surface-A + HS. The "c" indicates that the subject has made a successful attempt to identify the case that contains the comparison surface, and "i" indicates a failed attempt.

standard deviation shows the largest difference in the average threshold of each subject. The standard error is indicative of far away is the experimental mean from the unbiased population mean.

As seen in Figure 4.4a and Table 4.1, the effect of speed on sensitivity is not very distinct due to the large variation between subjects. However, in Table 4.2, it is shown that there are 50% to 83% of the subjects who exhibit the trend of a decrease of sensitivity when increasing speed at certain points in their experiments.

According to Table 3.1, the continuous force output of the Phantom Desktop is rated at 1.75N, and the average applied force from numerous subjects were higher than this rating,

		Speed (mm/s)		
		70	120	200
Surface-A (86.8 mm)	Mean	60.7	50.9	75.0
	Standard Deviation	29.5	24.2	20.1
	Standard Error	8.51	6.99	5.81
Surface-B (148 mm)	Mean	68.1	74.3	76.1
	Standard Deviation	42.9	20.3	24.7
	Standard Error	12.4	5.87	7.13

Table 4.1: Statistical results of Experiment One. (Results are in % difference)

Surface	Trend	Number of Subjects
Surface-A	$JND_{LS} < JND_{MS}$	7
	$JND_{MS} < JND_{HS}$	10
	$JND_{LS} < JND_{HS}$	7
Surface-B	$JND_{LS} < JND_{MS}$	7
	$JND_{MS} < JND_{HS}$	8
	$JND_{LS} < JND_{HS}$	6

Table 4.2: Number of subjects exhibiting the trends of decrease of JND with increase of speed

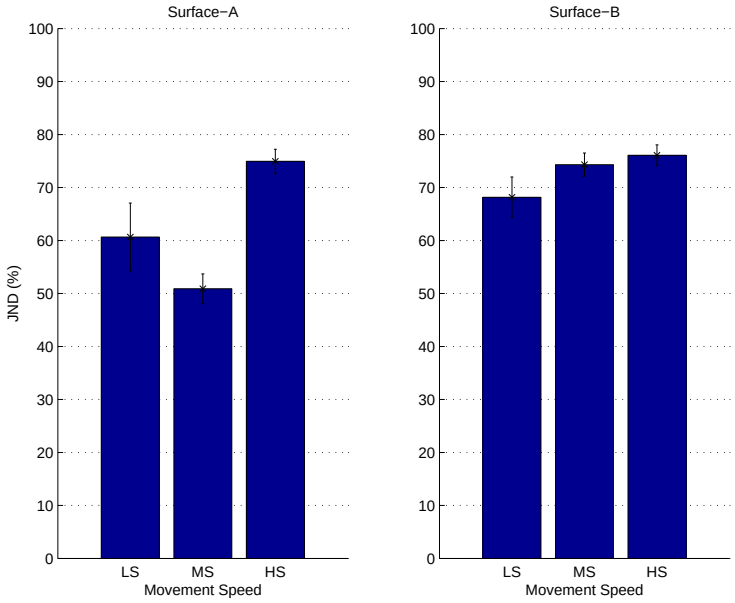

(a) The JND values for each surface and speed along with standard errors

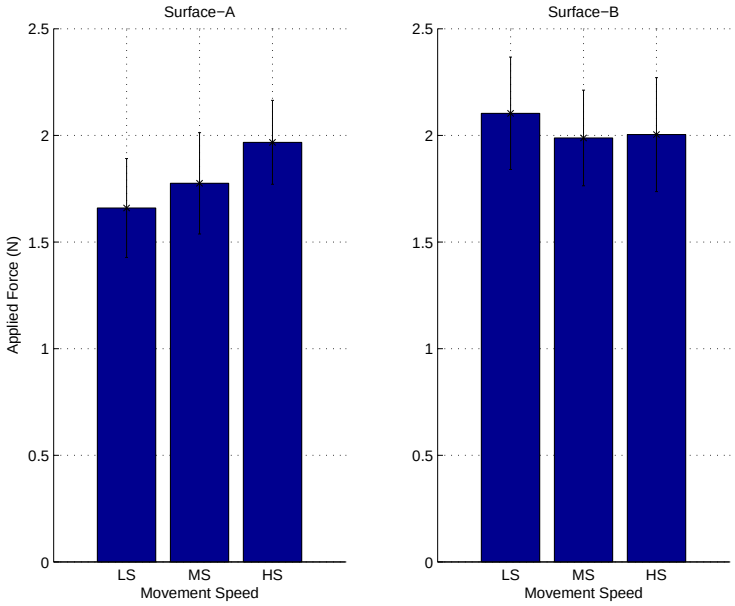

(b) Average applied force for each surface and speed with standard errors

Figure 4.4: Results of Experiment One

Speed (mm/s)	Just Noticeable Difference (%)	
	<Avg. Force	>Avg. Force
70 (Low Speed)	59.1	73.0
120 (Medium Speed)	61.7	67.6
200 (High Speed)	71.5	78.2

Table 4.3: Average sensitivity sorted by average applied force

as seen in Table A.3 and Figure 4.4b. When the Desktop device cannot continuously sustain the reaction force to achieve high-stiffness, then it will either decrease the force output or cut the feedback to protect itself from overheating. This means that the model the subjects feel when applying too much force is "softer" than expected. To counter this phenomenon, the following analysis separates the data by the average force applied during the experimentation.

The sensitivity data are sorted according to the mean force applied by the subjects for each experimental set, and then they are split into two equally-divided groups – data[1] with mean applied force lower than the median[2] of the experimental sets' forces and those that are higher. By plotting the average sensitivity data of each group, a distinguishable trend can be seen in the group of data with lower applied force, as see in Figure 4.5(separated by experimental sets and applied forces) and Figure 4.6 (separated only by applied forces).

After analyzing the sorted data with analysis of variance (ANOVA), the results (shown in Table A.2) show that the speed significantly affects the sensitivity with $F(2, 22) = 6.676, p = 0.005$ (with cutoff set at 0.05). The difference in surface curvature and the interactions between the curvature and speed have no significant effects on the sensitivity

[1]Subjects tend to have apply different amount of force for each of the six experimental sets. Therefore the data are sorted by individual experimental sets, not by subjects.

[2]The median of the force is used to produce even-sized groups.

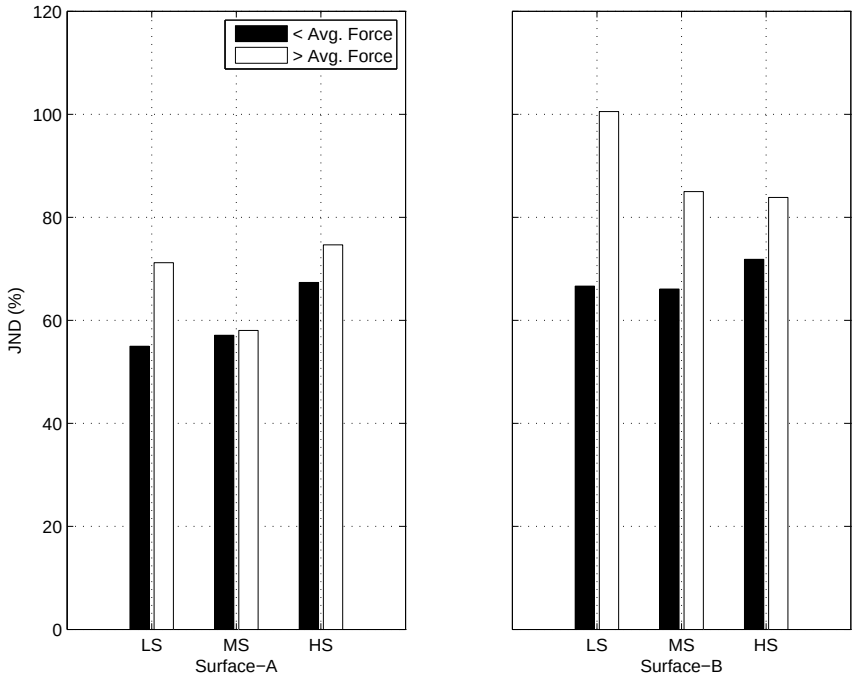

Figure 4.5: The JND for data with lower applied force and data with higher applied force

with $F(1, 11) = 0.914, p = 0.360$ and $F(2, 22) = 2.306, p = 0.123$ respectively.

4.5 Conclusion

The analysis shows that as the speed of the subject's hand increases, the JND for the change in surface resolution increases as well (decrease of sensitivity). For the speeds 70 mm/s, 120 mm/s and 200 mm/s, the average JND are 59.1% , 61.7%, and 71.5% change for x and θ respectively for high-resolution models. Even though the average trend is visible, the threshold values for each individual can differ greatly from one another. As Zadeh [49] has pointed out, to accurately implement this effect in compression techniques, individual calibrations are required to match force sensitivity with the user's speed in the algorithm for velocity-driven haptic feedback.

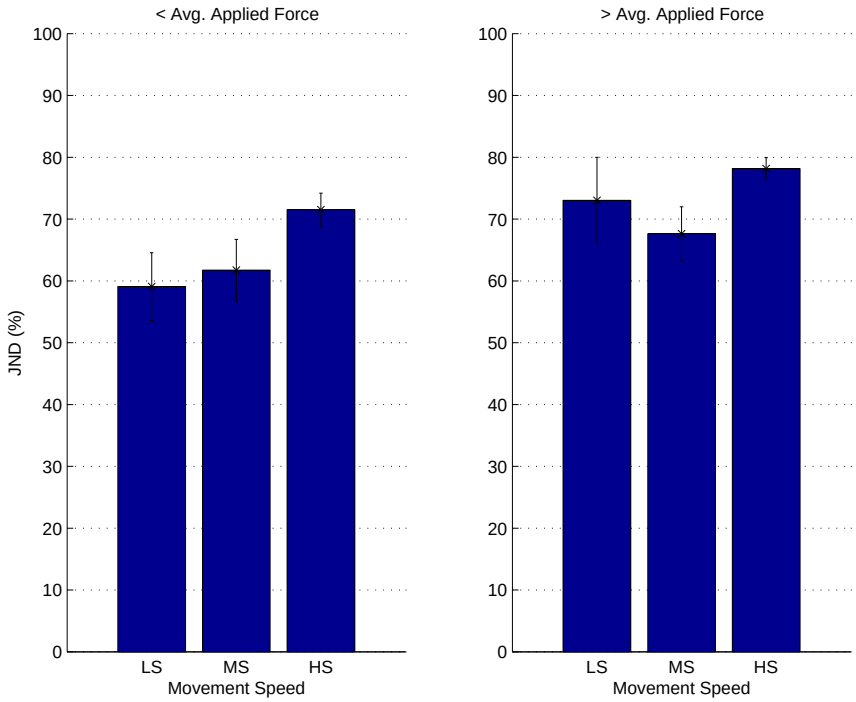

Figure 4.6: Mean JND data for results grouped by applied forces.

The results have also shown that the average sensitivity is lowered and unpredictable trends can occur when the applied force is higher than the rated continuous force of the device. This is speculated that the reaction force cannot be accurately generated by the device when the force output is at its limits. The device will generate the maximum force it can sustain, which will be lower than the required reaction force. This can cause discretions when subject is trying to sense the difference.

For the results with lower applied forces, the results confirm Hypothesis H_1.

Chapter 5

Experiment Two: JND of Declination

The objective of this experiment is to determine the just noticeable difference (JND) of surface with changes of larger surface detail with respect to the user's movement speed. The subject is asked to feel the haptic surface with a constant resolution at each determined speed. This experiment shall determine the threshold where the subject can not distinguish the difference in magnitude of angular change between two surfaces.

5.1 Hypothesis

The hypothesis tested in this experiment is stated as follows:

> H_2: The JND of human perception on angular change increases when the movement speed of the user's hand increases in a haptic environment with models.

The hypothesis for this experiment is motivated by the velocity-driven multiresolution haptic compression technique developed by Kolčárek[23] and the results from Experiment One. In experiment one, the reduction of resolution changes both the length of each

face and the angular difference between two faces (evidently shown in Table B.1). This experiment investigates whether the change in sensation dependent purely on the angular difference or not by keeping the length of the face at a constant.

5.2 Method

Using the virtual environment described in Chapter 3, two haptic surfaces are selected to be the standard surfaces used in the Forced-Choice Tracking (FCT) measurement. Both surfaces have the highest stiffness setting allowed by the haptic device, the PHANToM Desktop. The subjects are trained to feel the surfaces at the three average speeds specified in Section 3.4.2: 70 mm/s, 120 mm/s, and 200 mm/s.

The two standard surfaces are given with the shape of isosceles trapezoids, with the angles θ being 10° (Surface-A) and 5° (Surface-B), as defined in Figure 5.1. Figure 5.2 is a screenshot of the surface implemented in the test. The trapezoidal shape can be related to a low-resolution representation of cylindrical curves, as the radius of curvature R is defined in Equation 5.1, where x is the length of the horizontal face on top. In this experiment, $x = 0.0243$ m, which holds true for both standard surfaces and their subsequent comparison surfaces.

$$R = \frac{x}{2}\tan\left(\frac{180^\circ - \theta}{2}\right) \tag{5.1}$$

The comparison surfaces in each experimental set are created by changing the angle θ. The angular difference between the standard surface and comparison surfaces starts off with a 50% increase from the standard angle in the FCT procedure. The comparison angle is always larger than the standard angle. When the stimulus-changing criteria are met, the difference between SS and CS angles are varied by 30%. For example, if the subject makes an incorrect choice when the difference is 50%, then the difference is increased to

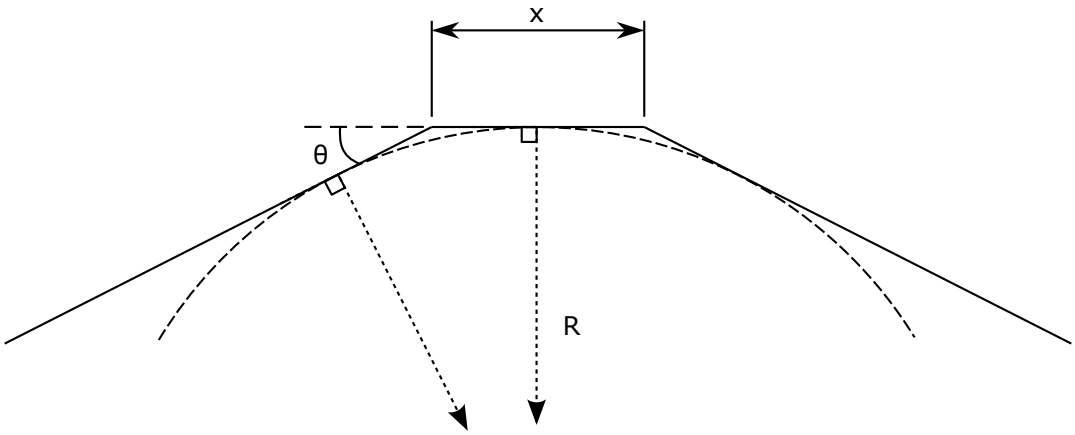

Figure 5.1: The definition of the isosceles trapezoid used in this experiment with respect to θ. The relationship between the trapezoidal surface and a cylindrical curve can also be seen here.

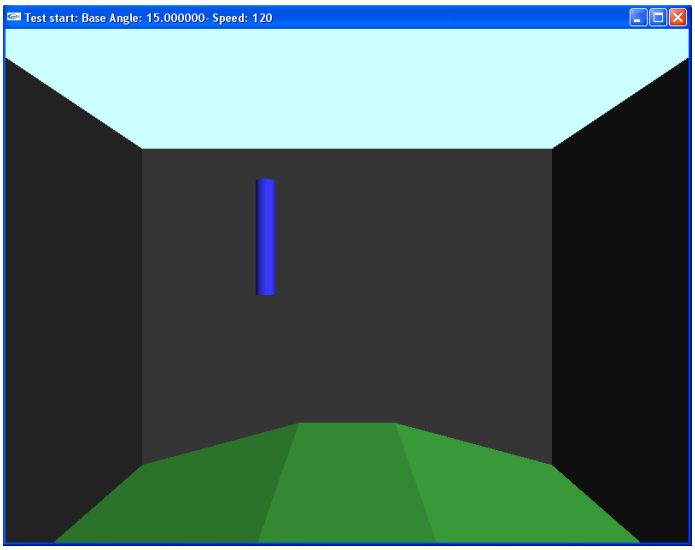

Figure 5.2: A screenshot of the trapezoidal haptic surface with $\theta = 10°$ in the experimental phase

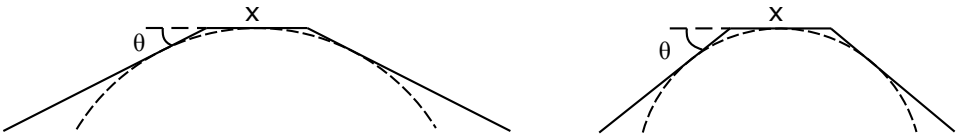

Figure 5.3: Decrease of curvature due to increase of θ

65%; if the correct criterion is met, then the difference is decreased to 35%. As illustrated in Figure 5.3, the changing of the angle θ is inversely propotional to the changing of the radius of curvature the surface represents.

5.3 Participants

The participants were selected from the general student body, with a total number of 17, with 5 of whom returned from the first experiment. The participants' were aged between 18 to 25, and had either no experience with haptic devices or less than 5 hours. Only one of the subjects was left-hand dominant, while all others were right-hand dominant. None of them had any known muscular disease or injuries in their arms. There were 35% of females and 65% of males. All of them were familiar with a 3D virtual environment. The University of Waterloo office of research approved the experiment as Research Involving Human Participants (ORE #16157). The experiment was conducted in accordance with the University of Waterloo ethical guidelines. Signed consent letters are obtained from all participants prior to the experiments.

5.4 Results

The results from the 17 subjects are given in Table A.4 in Appendix A. A sample result from the test case Surface-A + HS is given in the forced-choice tracking plot in Figure 5.4. The results are taken from the average of the last 15 trials of each test case, where the

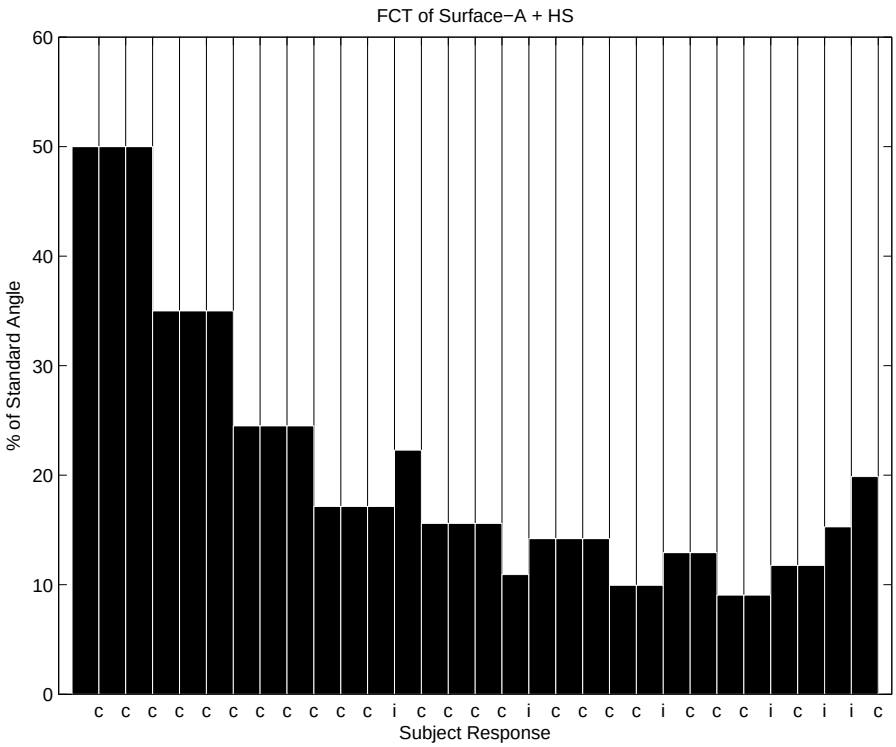

Figure 5.4: A sample FCT plot for Surface-A + HS. The "c" indicates that the subject has made a successful attempt to identify the case that contains the comparison surface, and "i" indicates a failed attempt.

JND is the percentage-difference between the threshold angle and the standard angle. The statistical result from all subjects are shown in Table 5.1, and a graphical representation of the data is shown in Figure 5.5a.

The effect of speed on sensitivity can be seen in Figure 5.5a and Table 5.1. Even though the trends are much more visible in this experiment than the previous one in Chapter 4, the average applied forces are still higher than the maximum rated continuous force output from the haptic device, as seen in Table A.6 and Figure 5.5b. To be consistent with the analysis, the data are sorted by the amount of applied forces also. The results calculated after sorting is given in Table 5.2 and Figure 5.7.

		Speed (mm/s)		
		70	120	200
Surface-A (5°)	Mean	22.8	19.2	15.3
	Standard Deviation	8.63	9.62	7.95
	Standard Error	2.09	2.33	1.93
Surface-B (10°)	Mean	27.8	19.6	18.0
	Standard Deviation	8.19	8.98	7.95
	Standard Error	1.99	2.18	1.93

Table 5.1: Statistical result of Experiment Two. (Results are in % difference)

	Just Noticeable Difference (%)	
Speed (mm/s)	<Avg. Force	>Avg. Force
70 (Low Speed)	28.6	29.2
120 (Medium Speed)	24.6	24.5
200 (High Speed)	19.7	21.9

Table 5.2: Average sensitivity sorted by average applied force

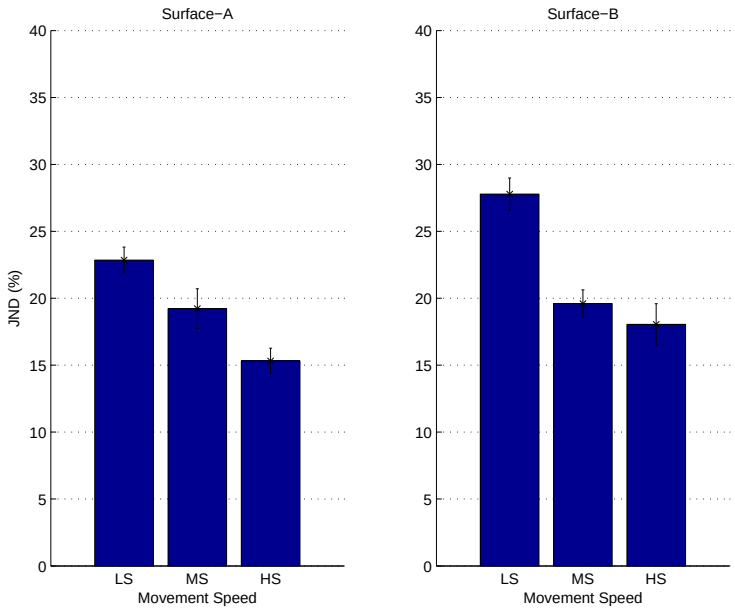

(a) Average % threshold

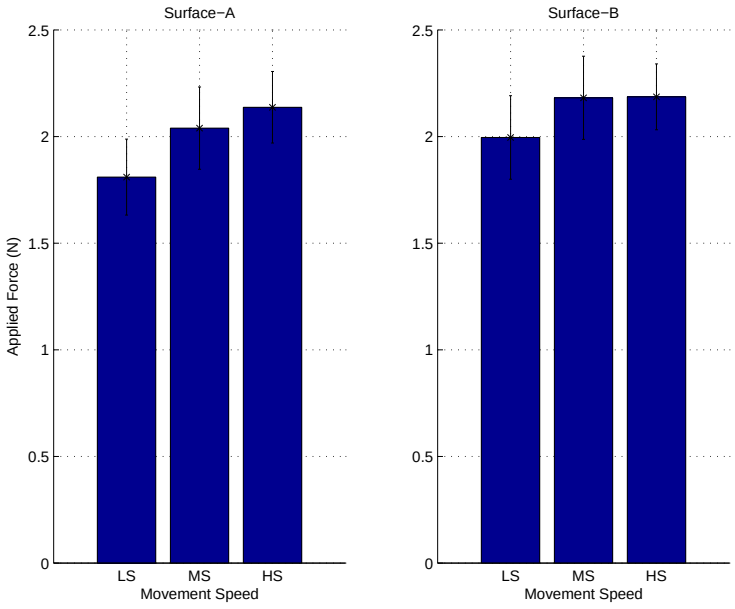

(b) Average applied force

Figure 5.5: Results of Experiment Two

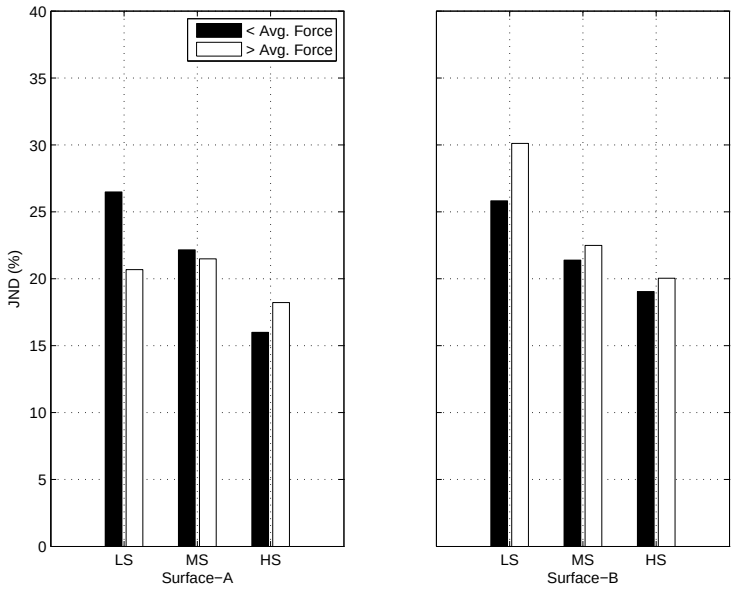

Figure 5.6: JND after sorting by applied force

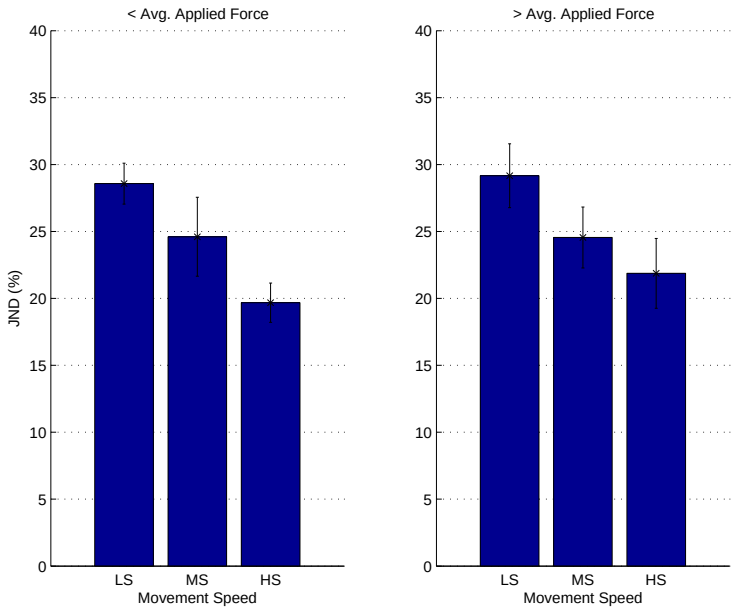

Figure 5.7: JND after sorting by applied force

With the analysis of variance (ANOVA), the results (shown in Table A.5) show that the speed significantly affects the sensitivity with $F(2, 32) = 3.766, p = 0.034$ (with cutoff set at 0.05). The difference between the standard angles and the interactions between the surface and speed have no effects on the sensitivity data with $F(1, 16) = 0.927, p = 0.350$ and $F(2, 22) = 2.149, p = 0.133$ respectively.

5.5 Conclusion

The analysis shows that as the speed of the subject's hand increases, the JND for the change in the declination of the angle θ for a trapezoidal surface decreases. For the speeds 70 mm/s, 120 mm/s and 200 mm/s, the average JND are, respectively, 22.8%, 19.2%, and 15.3% changes for $\theta = 10°$, and 27.8%, 19.6%, and 18.0% changes for $\theta = 5°$.

The JND trends shown in both surfaces are the exact opposite as hypothesized. The JND for changes in angular difference between faces decreased as the movement speed increased. The magnitude of the applied force does not seem to affect the outcome as well. This experiment contradicts the hypothesis H_2.

With speed of motion having the opposite effect on the JND of angular change between two surfaces, a couple of studies on curvature sensing may produce a plausible explanation.

When tracing a curvature with hand, a law in motor psychophysics states that the tangential speed (v) is one-third power of the curvature of the path (R) multiplied by constant (K), shown in Equation 5.2 [24]. This law measures estimates the average speed. However, this appears to only affect the low-level sensorimotor processes, but not the high-level motion planning process for haptics [48].

$$v = K \cdot R^{\frac{1}{3}} \tag{5.2}$$

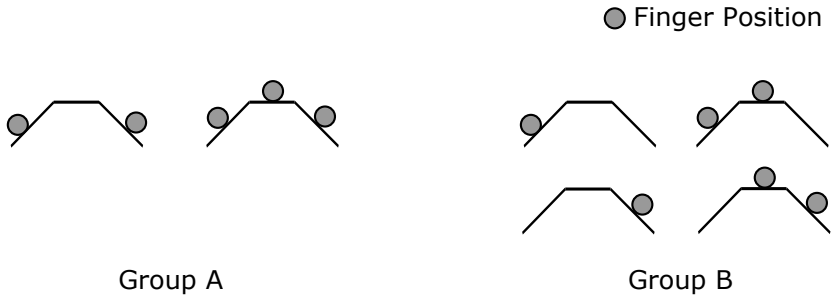

Figure 5.8: Different finger configurations in Pont's experiment [33].

Pont et al. have studied the JND of curvature differentiation by fingertips with both static and dynamic touch in [33]. The experiment with static touch investigates how well a person can differentiate curvatures by placing only the tips of one, two, or three fingers statically on a surface with an unknown curvature. The different configurations of finger placements used in the experiment with trapezoidal surface are shown in Figure 5.8. Their results show that the JND of Group A configuration is much lower than Group B. It is concluded that the human hand differentiates curvatures by the height and *local attitude*(tangential angle) differences felt by each finger. Also, the resulting sensitivity for a curved surface is very similar to the results for the trapezoidal surface.

In the experiment with dynamic touch, Pont et al. investigated curvature discrimination with one finger moving across curved surfaces with different lengths (constant curvature). The subjects are required to feel the entire length of the curve. The increase of surface length contributes to the increased difference in height and attribute from end to end, shown in Figure 5.9. The results show an decrease in JND with the increase of surface length. However, in the experiments conducted, there are no mention of the speed in which the subjects moved to feel the curved surface. The findings in this experiment are confirmed by Wijntjes et al. with a robot that can reproduce the surface height and orientation of a curve with the user's horizontal position [47].

In the experiment conducted in this chapter, subjects are instructed to feel the trape-

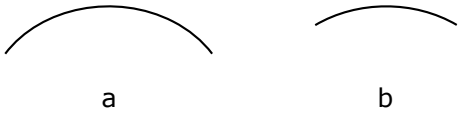

Figure 5.9: Two curves with same curvature but different length

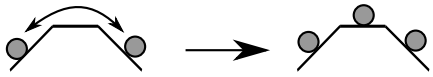

Figure 5.10: By moving the point of contact at a high enough speed, then the multi-finger touch configuration may be achieved.

zoidal surface at different speeds. Given a fixed time-frame, the length traversed by the slower speed is always shorter than the faster speed. With Pont's and Wijntjes' findings, it is suspected that the trends exhibited in Experiment Two is due to the humans are more sensitive to change of curvature than change of surface resolution. For a single-point contact such as the haptic device used in this experiment, it is speculated that, when the speed of the subject's hand is sufficiently high, then it is possible to achieve the heightened sensitivity as seen in the Group A configuration. Figure 5.10 illustrates such a situation.

This behaviour may possibly be attributed to the sensitivity of curvature being higher than sensitivity for resolution. To confirm this hypothesis, further testing is required. Suggestions are made in Section 6.1 for possible tests.

Chapter 6

Conclusion and Future Research

This thesis presents a study of the just noticeable difference of haptic sensations relative to the speed of the user's hand movement. Two experiments were designed to determine how the speed affects the user's ability to sense (1)changes of small surface detail with a multiresolution model of constant radius of curvature and (2)changes of large surface geometry with a low-resolution models of varying radius of curvature.

In the first experiment, two high-resolution cylindrical surfaces with different curvatures are used to measure the subject's sensitivity to the change of resolution in relationship to the speed of the subject's arm. The findings show that, as long as the subject does not apply a force that exceeds the rated force of the device, the sensitivity for small and dense changes decreases as the speed increases. This means that, at a high speed, the level of detail can be decreased without the subject noticing the change. Furthermore, the statistical analysis suggests that the curvature has insignificant influence on the relative sensitivity for the resolution change.

In the second experiment, a low-resolution trapezoidal model is used to measure the subject's sensitivity to angular changes at different speeds, and two starting angles are provided. As the results show, regardless of the forces applied, the subject is more sen-

sitive to the angular change at high speed than at low speed. This created an appeared contradiction with the results from the first experiment. There is some literature that may partially support the findings, but further investigations are needed to fully explain the trend. The results are indications that reducing LOD with an increase of speed may not be optimal for all situations.

In conclusion, when a velocity-driven multiresolution compression technique is implemented, there are limits as to how much the level of detail of each model can differ from one another. For changing the surface resolution without changing its curvature, the JND of resolution change increases with movement speed. When the angular difference of a trapezoid is changed without changing its resolution, the JND for angular change decrease with increasing movement speed. This indicates that the curvature of the surfaces may have to be preserved for all different levels of detail for the same model. The resolution of smooth cylindrical surface can be reduced up to 65% without the user detecting any difference. A 10% decrease of resolution was observed when the movement speed went from low (70 mm/s) to high (200 mm/s). For a high-resolution model (in the range of thousands to tens of thousands of vertices [18]), a 10% reduction means hundreds of vertices can be eliminated from the calculation. However, if changing the number of vertices may lead to changing the curvature, then the algorithm should refrain from making those changes while the user is in contact with the model.

6.1 Future Recommendations

For future studies, several experiments can be performed to complement the findings of this thesis. Most importantly, to verify the findings of Experiment Two, the sensitivity of curvature change should be thoroughly investigated. The high-resolution surface from Experiment One can be modified for this purpose. Instead of changing resolution, having

the cylindrical surface changes its curvature for the comparison surface for each trial will give better insights into sensitivity to changes of surface curvature.

A study of concave surfaces should be conducted in a similar manner as this research, since the experiments performed here have all used convex surfaces. Models with concave sections may end up with a different type of compression technique than the convex sections to maintain the same sensation.

Also, this research has required only one type of motion from its subjects, but haptic simulations do not commonly restrain the motion of their users. It is possible that the sensitivity JND's measured in this research are only associated with the motion of moving the arm left and right. A full comprehensive study should be conducted by having the subject feel the haptic model in a range of motion, including unrestricted motion.

The relationship between voluntary applied forces and haptic sensitivity should be thoroughly investigated. The sensitivity of subject should be tested with different levels of applied forces. A haptic device with higher force capabilities should be considered for this experiment to separate mechanical limitations and loss of sensitivity. With higher force output, the feedback forces can be more accurately generated, and thus the loss of sensitivity due to higher movement speed may be observed more clearly. The Delta robots mentioned in Section 2.1 have a much higher force output than the anthropomorphic robots.

This experiment uses models with highest spring-damper stiffness in the force calculation, so the relationship between speed and sensitivity may result differently if the model has been softer or even deformable. Possible control groups may contain fixed-vertex models with various values for the spring-damper constants.

This thesis investigated the multiresolution technique for compression of surface models with high-stiffness, but there is also a significant portion of the haptic research that is dedicated to deformable models with much more accurate reaction forces. Those models are constructed with a truss-structure with internal vertices, and each connection between

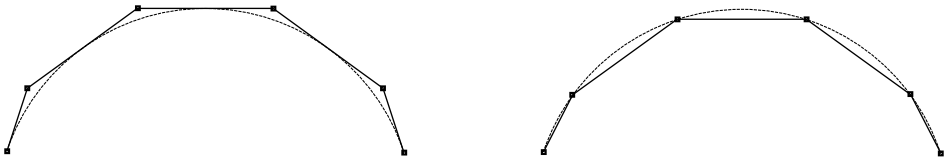

Figure 6.1: Different methods of defining the vertices of a model. The left model is defined by the tangent lines of the curve, whereas the right model is defined by the points lying on the curve. Changing the resolution of the right model changes the perceived curvature, but the left model is unaffected.

vertices is a spring-damper system. As one can imagine, this makes the computation much more complicated than pure surface models. If a velocity-driven multiresolution structure can be introduced into these models, it may significantly reduce number of calculations.

Model compression is not purely about reduction of data storage; it is also about preserving the perceived level of details for the user. The results from this research have shown that reduction of model resolution with increase of user speed is effective under the premise that the changes do not affect the curvatures of the model. This means that the vertices of the model can not simply be points on the modeled surface, but rather the intersection points of the tangential planes (shown in Figure 6.1). Changing the number of tangential planes (resolution) does not affect the curvature of the model.

Unfortunately, the haptic model compression is not applicable to all applications, such as ones involving generating haptic effects such as tactile feedback or vibration, where virtual models are not needed. Haptic applications involving realistic model detail and interaction can benefit the most haptic compression, such as surgical simulation. In surgical simulation, the user has to work with non-conventional model shapes such as the muscle or organ tissues [2]. Those models have to be deformable and highly-detailed to closely reflect their real-life counterparts. Even though the operations performed on those models are also complex to simulate (such as cutting [42] and needle insertion [29]), their area of

operation is usually considerably smaller than the size of the models. In which case, local detail is more stressed than overall model detail.

For vision, movement is only one of many factors that drive a compression algorithm. Many of those factors, such as distance and focus, can also be used for haptic model compression with modifications. For instance, parts of the haptic model that are out of the workspace of the haptic device can be culled, just like how visual rendering process cull models outside of the viewport. For a deformable model, there may be psychophysical methods to reduce the densities of internal vertices at certain parts of the model to simplify the calculations as well. Different psychophysical factors and their combinations should be investigated. When model compression technique is implemented correctly, the designer for the haptic environments has much more freedom to create complex models with realistic effects, thus enhancing the haptic experience for the user.

Appendix A

Experimental Results

Subject	JND (%-diff)					
	Surface-A			Surface-B		
	LS	MS	HS	LS	MS	HS
CH	31.8	46.2	65.4	52.2	81.0	30.4
AL	29.2	37.7	48.0	61.3	48.0	76.4
DB	24.0	96.9	79.1	54.0	79.1	49.6
NM	99.0	94.7	76.3	138.1	66.9	64.8
RC	106.0	48.0	69.1	168.7	119.6	110.8
RK	78.1	30.4	66.2	71.6	41.7	83.5
KW	60.2	46.5	49.6	79.8	63.0	72.2
MA	84.7	26.9	82.8	42.7	62.8	57.3
PC	26.4	55.0	22.4	38.9	71.4	67.3
DW	50.8	37.3	68.6	57.9	68.6	77.1
AH	54.3	57.3	96.6	110.8	72.0	73.0
CB	69.5	77.1	80.1	62.2	80.1	116.6

Table A.1: Resulting JND from Experiment 1.

Source	Type III SS	DF	Mean Sq.	F	Prob >F
Speed	7.437e3	2	3.718e3	6.676	0.0054
Error	1.225e4	22	557.1		
Surface	5.782e2	1	5.782e2	0.914	0.360
Error	6.959e3	11	632.7		
Speed*Surf	2.655e3	2	1.328e3	2.306	0.123
Error	1.266e4	22	575.6		

Table A.2: ANOVA Table for Speed and Surface

Subject	Applied Force (N)					
	Surface-A			Surface-B		
	LS	MS	HS	LS	MS	HS
CH	1.974	2.028	1.749	1.963	2.427	2.195
AL	0.376	0.439	0.650	0.358	0.439	0.533
DB	0.706	1.207	2.481	2.298	1.301	1.957
NM	2.681	2.668	2.709	2.757	2.203	3.136
RC	2.953	3.109	2.866	3.397	2.783	2.982
RK	1.088	1.156	1.418	1.205	1.409	1.215
KW	2.380	2.509	2.510	3.207	2.998	3.199
MA	0.851	0.684	0.890	1.151	0.960	1.101
PC	1.502	1.255	1.880	1.252	1.881	0.978
DW	2.515	2.745	2.476	3.157	2.633	3.287
AH	1.505	1.911	1.731	2.210	2.015	1.493
CB	1.384	1.593	2.250	2.288	2.802	1.966

Table A.3: Average applied force from Experiment 1.

Subject	JND (degrees)					
	Surface-A			Surface-B		
	LS	MS	HS	LS	MS	HS
DM	6.26	6.54	6.72	12.08	12.66	11.58
PC	6.11	6.11	5.73	11.58	11.10	11.24
RX	5.80	5.79	5.80	12.21	11.45	10.85
CW	6.44	6.10	5.92	12.34	12.11	11.31
ZL	6.15	5.72	5.51	12.54	11.38	11.35
BH	7.29	6.18	6.52	12.67	11.84	12.36
DW	6.57	5.96	5.86	11.17	11.78	11.48
FH	6.83	6.45	5.81	13.61	14.01	11.88
TL	6.72	5.96	6.01	11.95	13.72	12.84
VC	6.83	6.75	6.74	14.01	12.89	12.18
CB	5.81	5.91	5.72	12.36	11.57	11.13
KW	6.64	5.76	5.77	11.10	11.55	11.41
EW	6.63	7.49	6.40	12.83	14.15	13.80
LG	6.28	5.97	6.04	13.04	11.80	11.31
MA	6.51	5.96	6.61	12.34	13.15	13.04
CT	6.55	5.99	5.77	12.16	11.82	11.66
MK	6.30	6.43	6.19	12.78	11.65	12.19

Table A.4: Resulting JND from Experiment 2.

Source	Type III SS	DF	Mean Sq.	F	Prob >F
Speed	608.010	2	304.005	3.766	0.034
Error	2583.1	32	80.721		
Surface	69.725	1	69.725	0.927	0.350
Error	1203.3	16	75.205		
Speed*Surf	303.743	2	151.872	2.149	0.133
Error	2261.9	32	70.6853		

Table A.5: ANOVA Table for Speed and Surface

Subject	Applied Force (N)					
	Surface-A			Surface-B		
	LS	MS	HS	LS	MS	HS
DM	2.030	2.836	2.346	2.348	3.170	2.849
PC	3.238	3.180	2.182	1.635	1.704	1.274
RX	2.503	2.490	3.117	2.448	3.012	2.497
CW	1.328	1.264	1.599	1.366	1.552	1.458
ZL	1.268	1.672	1.814	0.720	1.306	2.203
BH	1.944	2.131	2.918	2.519	2.913	3.244
DW	2.249	1.757	3.112	3.302	2.342	2.156
FH	2.331	3.544	2.544	2.698	2.885	2.742
TL	1.918	2.473	2.757	3.545	1.852	1.745
VC	1.353	1.467	1.430	1.578	2.259	3.050
CB	1.261	1.134	1.862	0.847	1.111	1.919
KW	2.865	2.596	2.886	2.472	3.597	2.927
EW	1.049	1.634	2.197	1.623	1.523	1.696
LG	2.602	3.018	2.114	2.235	3.181	2.731
MA	0.488	0.724	0.572	0.774	0.842	1.122
CT	0.864	1.108	1.284	2.292	1.556	1.707
MK	1.477	1.644	1.599	1.523	2.284	1.842

Table A.6: Average applied force from Experiment 1.

Appendix B

Surface Properties of Experiment One

30-n	Surface-A		Surface-B		% Difference
	x (mm)	θ (rad)	x (mm)	θ (rad)	
0	3.802	0.022	3.613	0.012	0.0
1	3.933	0.023	3.738	0.013	3.4
2	4.073	0.023	3.872	0.013	7.1
3	4.224	0.024	4.015	0.014	11.1
4	4.387	0.025	4.169	0.014	15.4
5	4.562	0.026	4.336	0.015	20.0
6	4.753	0.027	4.517	0.015	25.0
7	4.959	0.029	4.713	0.016	30.4
8	5.185	0.030	4.928	0.017	36.4
9	5.432	0.031	5.162	0.017	42.9
10	5.704	0.033	5.421	0.018	50.0
11	6.004	0.035	5.706	0.019	57.9
12	6.338	0.037	6.023	0.020	66.7
13	6.711	0.039	6.377	0.022	76.5
14	7.131	0.041	6.776	0.023	87.5
15	7.607	0.044	7.228	0.024	100.0
16	8.151	0.047	7.745	0.026	114.3
17	8.779	0.051	8.341	0.028	130.8
18	9.512	0.055	9.036	0.030	150.0
19	10.379	0.060	9.858	0.033	172.7
20	11.420	0.066	10.845	0.037	200.0

Table B.1: Table of absolute values and percentage differences of face length x and angular difference θ.

References

[1] Mohammad Waqas Asghar and Kenneth E. Barner. Nonlinear multiresolution techniques with applications to scientific visualization in a haptic environment. *IEEE Transactions on Visualization and Computer Graphics*, 7(1):76–93, 2001. 4

[2] Daniel Bielser and Markus H. Gross. Open surgery simulation. 2002. 80

[3] J. Duchateau C. Balestra and K. Hainaut. Effects of fatigue on the stretch reflex in a human muscle. In *Electroencephalography and Clinical Neurophysiology/Evoked Potentials Section*, volume 85, pages 46–52, 1992. 36

[4] Paul Chandler and John Sweller. Cognitive load theory and the format of instruction. In *Cognition and Instruction*, volume 8, pages 293–332, 1991. 43

[5] Megan M. Cooper, Claudia Carello, and M. T. Turvey. Further evidence of perceptual independence (specificity) in dynamic touch. In *Ecological Psychology*, volume 11, pages 269–281. Lawrence Erlbaum Associates Inc., 1999. 1

[6] W.G. Darling and K.C. Hayes. Human servo responses to load disturbances in fatigued muscle. *Brain Research*, pages 345–351, 1983. 36

[7] Herve Delingette. Towards realistic soft-tissue modeling in medical simulation. In *Proceedings of the IEEE*, volume 86, pages 512–523, 1998. 19

[8] Force Dimension. omega.3, 2010. http://www.forcedimension.com/omega3-overview. 13

[9] David Feygin, Madeleine Keehner, and Frank Tendick. Haptic guidance: Experimental evaluation of a haptic training method for a perceptual motor skill. pages 40–47, 2002. 2

[10] Thomas A. Funkhouser and Carlo H. Séquin. Adaptive display algorithm for interactive frame rates during visualization of complex virtual environments. In *SIGGRAPH '93: Proceedings of the 20th annual conference on Computer graphics and interactive techniques*, pages 247–254, New York, NY, USA, 1993. ACM.

[11] George A. Gescheider. *Psychophysics The Fundamentals*. Lawrence Erlbaum Associates, Inc., 3rd edition, 1997. 25, 26, 28, 31, 32, 34, 35

[12] K.K. Gorowara. On bezier curves and surfaces. In *Aerospace and Electronics Conference*, volume 2, pages 754–756, 1988. 15

[13] A. Gregory, M.C Lin, S. Gottschalk, and R. Taylor. Fast and accurate collision detection for haptic interaction using a three degree-of-freedom force-feedback device. *Comput. Geom. Theory Appl.*, 15(1-3):69–89, 2000. 20

[14] Tan Kim Heok and Daut Daman. A review on level of detail. In *Proceedings of the International Conference on Computer Graphic, Imaging and Visualization*, 2004. 21

[15] P. Hinterseer, E. Steinbach, S. Hirche, and M. Buss. A novel, psychophysically motivated transmission approach for haptic data streams in telepresence and teleaction systems. pages 1097–1100, 2005. 4, 24

[16] Peter Hinterseer and Eckehard Steinbach. A psychophysically motivated compression approach for 3d haptic data. *Haptic Interfaces for Virtual Environment and Teleoperator Systems, International Symposium on*, 0:4, 2006. 4, 24

[17] John M. Hollerbach and David E. Johnson. Virtual environment rendering. In *Human and Machine Haptics*. MIT Press, 2000. 4

[18] Hugues Hoppe. Progressive meshes. In *SIGGRAPH '96: Proceedings of the 23rd annual conference on Computer graphics and interactive techniques*, pages 99–108, New York, NY, USA, 1996. ACM. 4, 78

[19] SensAble Inc. PHANTOM®Desktop™Haptic Device, 2010. http://www.sensable.com/haptic-phantom-desktop.htm. 12, 42

[20] SensAble Inc. PHANTOM®Omni™Haptic Device, 2010. http://www.sensable.com/haptic-phantom-omni.htm. 12, 42

[21] Hyun K. Kim, David W. Rattner, and Mandayam A. Srinivasan. Virtual-reality-based laparoscopic surgical training: The role of simulation fidelity in haptic feedback. volume 9, pages 227–234. informa healthcare, 2004. 2

[22] K. J. Kokjer. The information capacity of the human fingertip. *IEEE Trans. Syst. Man Cybern.*, 17(1):100–102, 1987.

[23] Pavel Kolcarek. *Multiresolution Methods for Haptic Rendering*. PhD thesis, Masaryk University, Brno, Czech Republic, 2006. 4, 5, 23, 53, 66

[24] Francesco Lacquaniti, Carlo Terzuolo, and Paolo Viviani. The law relating the kinematic and figural aspects of drawing movements. In *Acta Psychologica*, volume 54, pages 115–130, 1983. 74

[25] Marutomi Seiko Co. Ltd. HIRO III, 2010. http://www.maru-tomi.co.jp/. 14

[26] Tomas Moller and Eric Haines. *Real-Time Rendering*. A K Peters, Ltd, 3rd edition, 1999. 19

[27] Hugh B. Morgenbesser and Mandayam A. Srinivasan. Force shading for haptic shape perception. In *Proceedings of the ASME Dynamics Systems and Control Division*, volume 58, pages 407–412. ASME, 1996. 7

[28] Inc. Novint Technologies. omega.3, 2010. http://home.novint.com/. 13, 42

[29] A.M. Okamura, C. Simone, and M.D. O'Leary. Force modeling for needle insertion into soft tissue. In *IEEE Transactions on Biomedical Engineering*, volume 51, pages 1707 – 1716, 2004. 80

[30] Miguel A. Otaduy and Ming C. Lin. Sensation preserving simplification for haptic rendering. In *SIGGRAPH '05: ACM SIGGRAPH 2005 Courses*, page 72, New York, NY, USA, 2005. ACM. 4

[31] Walter R. Peters and Tina L. Bartels. Minimally invasive colectomy: Are the potential benefits realized? *Diseases of the Colon and Rectum*, 36(8):751–756, 2005. 2

[32] Sylvia C. Pont, Astrid M. L. Kappers, and Jan J. Koenderink. Anisotropy in haptic curvature and shape perception. *Perception*, 27:573–589, 1998. 5

[33] Sylvia C. Pont, Astrid M. L. Kappers, and Jan J. Koenderink. Similar mechanisms underlie curvature comparison by static and dynamic touch. *Perception & Psychophysics*, 61(5):874–894, 1999. 1, 5, 75

[34] Hong Qin and D. Terzopoulos. D-nurbs: a physics-based framework for geometric design. In *IEEE Transactions on Visualization and Computer Graphics*, volume 2, pages 85 – 96, 1996. 15

[35] Martin Reddy. *Perceptually Modulated Level of Detail for Virtual Environments*. PhD thesis, University of Edinburgh, 1997.

[36] Jr. Richard A. Damon and Walter R. Harvey. *Experimental design, ANOVA, and Regression*. Harper & Row, Publishers, Inc, 1st edition, 1987. 37

[37] Diego C. Ruspini, Krasimir Kolarov, and Oussama Khatib. The haptic display of complex graphical environments. In *SIGGRAPH '97: Proceedings of the 24th annual conference on Computer graphics and interactive techniques*, pages 345–352, New York, NY, USA, 1997. ACM Press/Addison-Wesley Publishing Co. 20

[38] SensAble Technologies. *OpenHaptics Toolkit: API Reference Manual*, 3.0 edition, 2008.

[39] SensAble Technologies. *OpenHaptics Toolkit: Programmer's Guide*, 3.0 edition, 2008. 9, 23

[40] Cyrus Shahabi, Antonio Ortega, and Mohammad R. Kolahdouzan. A comparison of different haptic compression techniques. 2002. 23

[41] Margaret H. Sharpe and Timothy S. Miles. Position sense at the elbow after fatiguing contractions. *Experimental Brain Research*, pages 179–182, 1993. 36

[42] Denis Steinemann, Matthias Harders, Markus Gross, and Gabor Szekely. Hybrid cutting of deformable solids. *Virtual Reality Conference, IEEE*, 0:35–42, 2006. 80

[43] Intuitive Surgical. The da vinci surgical system, 2005. http://www.intuitivesurgical.com/products/davinci_surgicalsystem/. 10

[44] CyberGlove Systems. CyberGrasp, 2010. http://www.cyberglovesystems.com/. 14

[45] Mechatronix Systems. FFS X NZFT, 2010. http://www.mechtronix.com/ffs-x-series/ffs-x-nzft/.

[46] E.H. Weber. *The Sense of Touch*. London: Academic Press, 1978. Translated by Translated by H.E. Ross and D.J. Murray from German orig. of 1834. 1

[47] M.W.A. Wijntjes, A. Sato, Vincent Hayward, and A.M.L. Kappers. Local surface orientation dominates haptic curvature discrimination. *IEEE transactions on haptics*, 2:94–102, 2009. 1, 5, 75

[48] A. Wing, C. Christou, and A. Waller. Touching trajectories: the relation between speed and curvature in exploring shape. In *Eurohaptics*, pages 76–79, 2001. 74

[49] Mehrdad Hosseini Zadeh, David Wang, and Eric Kubica. Perception-based lossy haptic compression considerations for velocity-based interactions. *MULTIMEDIA SYSTEMS*, 13(4):275–282, 2007. 5, 22, 63

[50] Mehrdad Hosseini Zadeh, David Wang, and Eric Kubica. *Factors Affecting the Perception-Based Compression of Haptic Data*, chapter 28. INTECH, 2010. 5

[51] Hongbin Zha, Yoshinobu Makimoto, and Tsutomu Hasegawa. Dynamic gaze-controlled levels of detail of polygonal objects in 3-d environment modeling. *3D Digital Imaging and Modeling, International Conference on*, 0:0321, 1999.

[52] Jian Zhang, Shahram Payandeh, and John Dill. Levels of detail in reducing cost of haptic rendering: A preliminary user study. In *HAPTICS '03: Proceedings of the 11th Symposium on Haptic Interfaces for Virtual Environment and Teleoperator Systems (HAPTICS'03)*, page 205, Washington, DC, USA, 2003. IEEE Computer Society.